$K^1\Lambda$ PHOTOPRODUCTION FROM HYDROGEN NEAR 90° IN THE CENTER OF MASS

Thesis by

J. Howard Marshall

In Partial Fulfillment of the Requirements

For the Degree of

Doctor of Philosophy

California Institute of Technology

Pasadena, California

1965

(Submitted May 27, 1965)

ACKNOWLEDGMENTS

I am particularly indebted to my partner in this experiment, Donald Groom. The care exhibited by him in the face of opposition from those wanting only speed made the difference between a functioning experiment and meaningless data. Few could have done as well as he.

The collaboration of Arpad Barna in the design and construction of the modular instrumentation system was most helpful. In addition, he provided valuable guidance in the design of reliable electronic circuitry.

The original idea to use a range telescope with a multidimensional pulse-height analyzer belonged to Professor Matthew Sands. In addition, his vast experience with instrumentation formed a basis for a demanding education provided me in the techniques of electronic design. That which I learned from him will not soon be forgotten.

After Professor Sands left Caltech for Stanford University, Professor Robert Walker became responsible for this experiment. His comments and suggestions and his support of the project are deeply appreciated.

The cooperation of Ransom Research in the design and fabrication of the Sampling Digitizer and in the production of parts of the modular instrumentation system is gratefully acknowledged. In particular, David Ransom, Sr., was most tolerant of the difficulties arising from a joint development project between an industrial concern and a university.

I also wish to thank Michael Hauser for his assistance in the accumulation of data and the staff and crew of the Synchrotron Laboratory for their cooperation. I am also indebted to the National Science Foundation for financial assistance during five years of my graduate work.

ABSTRACT

The differential cross-section for $\gamma + p \rightarrow K^+ + \Lambda$ has been measured for a center of mass angle of 90° and for photon energies between 1100 MeV and 1300 MeV. Range telescopes detected both the K^+ and the proton from the Λ decay. This experiment was performed in collaboration with D. E. Groom, who measured the polarization of the Λ hyperon in the above reaction. The electronic instrumentation for this experiment is emphasized here. The differential cross-section was found to remain nearly constant at $0.14 \pm 0.01 \mu b/sr$ over the above energy interval.

TABLE OF CONTENTS

TABLE OF CONTENTS (Cont'd)

LIST OF FIGURES

LIST OF FIGURES (Cont'd)

LIST OF TABLES

1.0 INTRODUCTION

Recently high energy physicists have discovered a confusing array of particles and resonances governed by laws which at present are only partly understood. One such resonance, $N^*_{1/2}(5/2^+, 1688)$, discovered in the pion-nucleon system, should be capable of decaying into $K^+ + \Lambda$. Therefore, the cross-section and polarization for the reaction

$$\gamma + p \rightarrow K^+ + \Lambda \qquad (1)$$

should be influenced by this resonant state.

The angular distribution of this cross-section has been measured at Cornell University[3,6,7,8,9] and at Caltech[1,2,4,5,10] for photon energies up to 1200 MeV. These data, which showed that for photon energies less than 1000 MeV the angular distribution was isotropic and the cross-section at 90° in the center of mass was proportional to the kaon center of mass momentum, implied that near threshold the production was nearly all in an s-wave state. However, at photon energies above 1000 MeV, the angular distribution started peaking in the forward direction, and the cross-section failed to be proportional to the center of mass momentum. Thus, higher partial-wave states had to be present in the production, and Anderson, et al.,[8] suspected the appearance of resonance effects at a photon energy of 1050 MeV, where the influence of the $N^*_{1/2}(5/2^+, 1688)$ would be strongest.

Extending these cross-section measurements to higher energies might test this possibility, while contributing to the general

knowledge of $K\Lambda$ photoproduction. For example, Daybell[11] measured the cross-section at backward angles for photon energies up to 1300 MeV and found continued departure from s-wave behavior. In addition, a measurement of the polarization of the associated Λ hyperon would provide independent data on the production amplitudes if more than one partial-wave state were present. Therefore, in 1960 it was decided to undertake the measurement of both the polarization and the differential cross-section at photon energies from 1100 MeV to 1300 MeV for center of mass angles near 90°, where the polarization was expected to be significant.

Because of the low synchrotron beam intensities available in 1960, an accurate polarization measurement was feasible only if the kaon detection efficiency could be increased over that obtained in previous successful cross-section experiments. The principal loss in efficiency in these experiments resulted from kaons decaying within magnets performing momentum selection. Also, the low solid angle of available magnets restricted the kaon counting rates. Therefore, a counter telescope was substituted for the magnetic spectrometer, with two additional telescopes for the detection of the Λ decay protons.

Because an earlier attempt with this technique[12] showed that statistical fluctuations in the rate of energy loss in scintillation counters and confusing events produced by nuclear interactions complicated the separation of kaons from numerous pions and protons, the final detection scheme had to consist of 28 counters, with pulse-height information being recorded from 18 of them. The

recorded pulse-heights were compared with the expected K^+ behavior by a digital computer in order to identify kaons unambiguously.

Donald E. Groom and I have collaborated on this experiment. Donald Groom, who has been primarily concerned with the design of the telescope and with the data analysis, was responsible for the Λ polarization data. It has been my task to develop the electronics and to report on the cross-section data. Beyond these broad outlines, no further division should be made between the efforts of Donald Groom and myself, because not all of his participation was restricted to the polarization experiment, nor all of mine to the cross-section measurement.

2.0 EXPERIMENTAL METHOD

2.1 General

Plan views of the experimental arrangement are shown in figure 1. A photon beam produced by bremsstrahlung from the electrons in the synchrotron was collimated, swept, and then passed through a liquid hydrogen target. Most photons were not absorbed by the target, but were collected by an ion chamber, which monitored the total energy of the beam. Particles produced in the target could enter the K- or Λ-telescopes, perspective drawings of which are shown in figure 2.

Because KΛ photoproduction is a two-body reaction, fixing the magnitude and direction of the kaon momentum determined all other kinematical quantities, including the photon energy. The K^+ Range Telescope defined both the kaon range and angle, thus establishing the plane of production and the energies involved. The two telescopes for detecting the decay proton from the associated Λ-hyperon were placed symmetrically above and below this production plane.

Four effects limited the kinematical region over which this kaon detection scheme could be applied. First, because at least 20 g/cm^2 of kaon range was required for clean particle identification (see Appendix A), the kaon kinetic energy had to exceed 140 MeV. Second, because of uncertainties in the absorption cross-sections for kaons in various materials, the kaon kinetic energy was limited to less than 450 MeV. Third, because counting rates increased rapidly as the angle of the K-telescope with the photon beam was

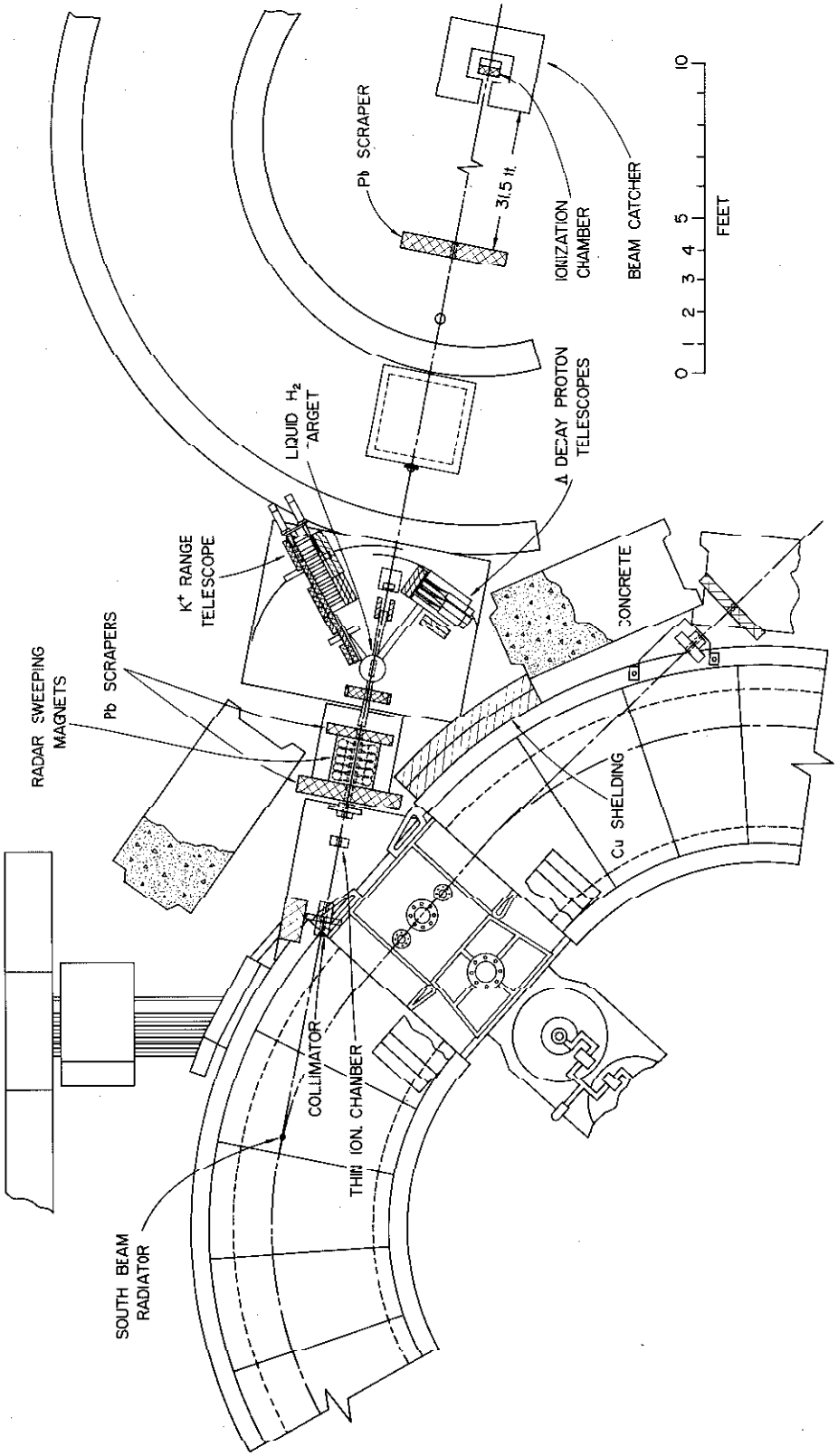

FIGURE 1a: Experimental Arrangement

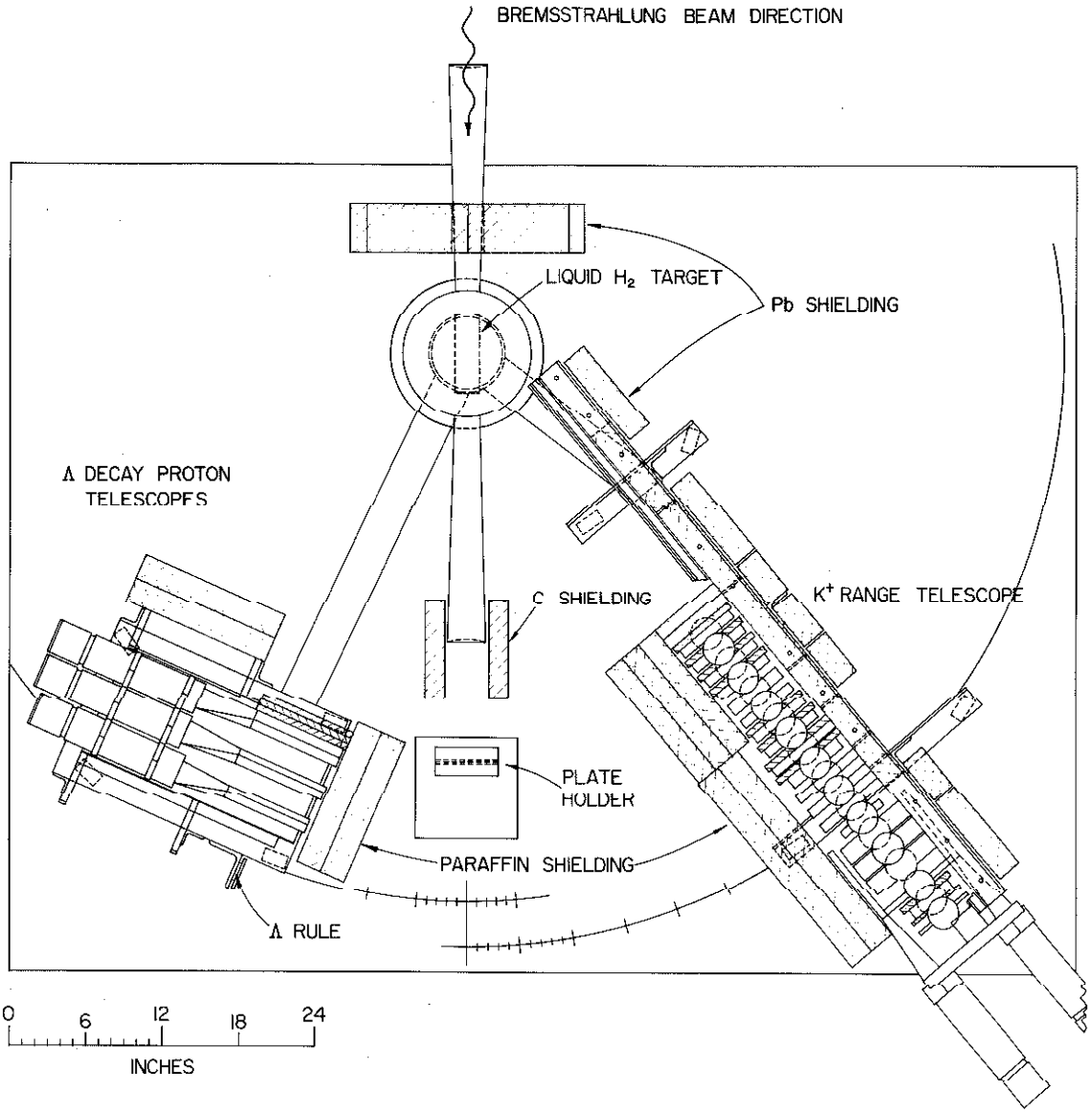

FIGURE 1b: Experimental Arrangement

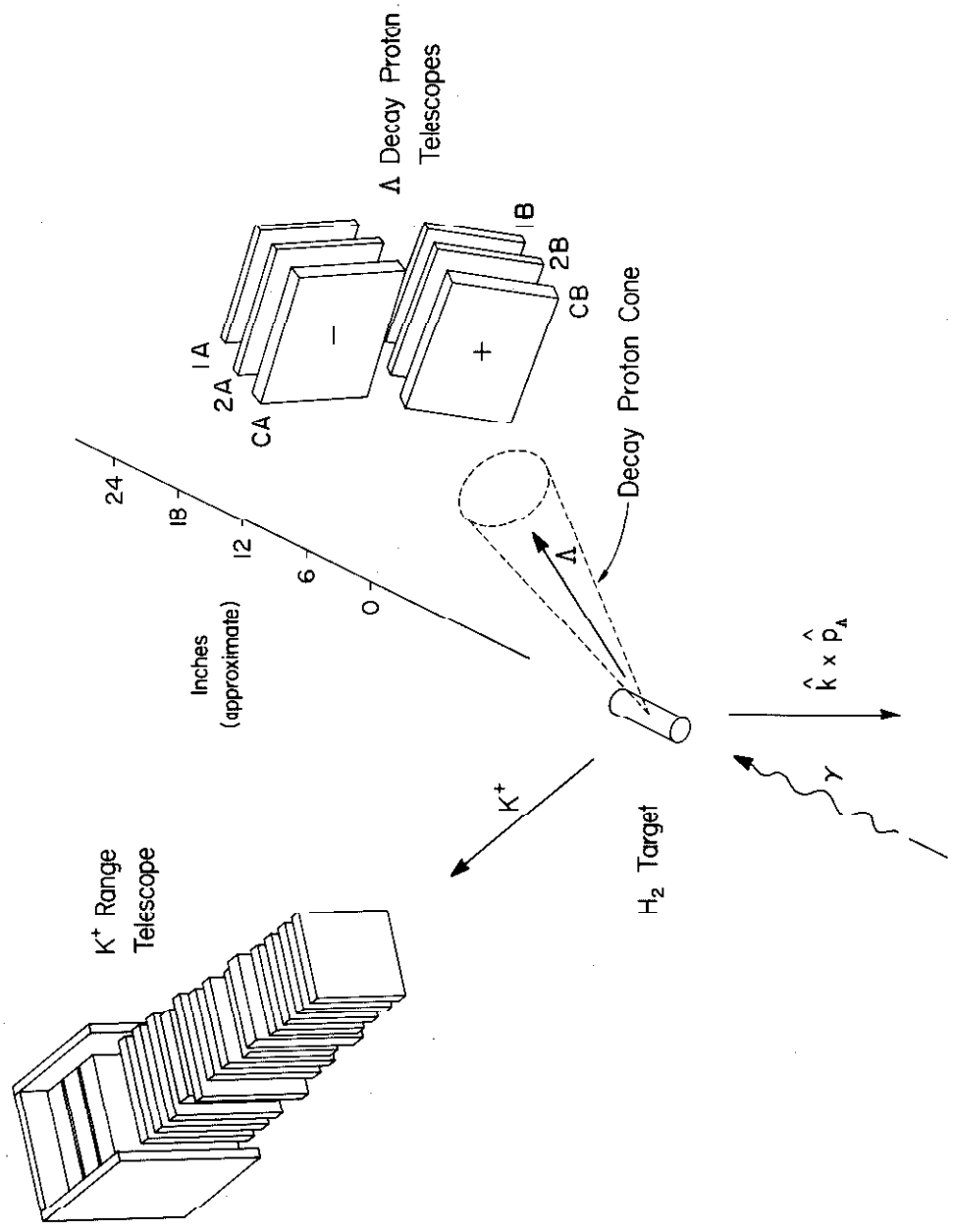

FIGURE 2: Perspective Drawing of the Telescopes

decreased, the counters were flooded for laboratory angles less than 25°. Fourth, because the maximum synchrotron end-point energy was about 1400 MeV, and because a strong dependence on the shape of the end of the bremsstrahlung spectrum was undesirable, the photon energy was limited to 1300 MeV or below. Therefore, it was decided to operate at a center of mass angle of 90° and at photon energies of 1100, 1200, and 1300 MeV. The same data provided both the differential cross-section and the Λ polarization.

2.2 Counter Telescopes

For the 1200 MeV point, the K-telescope (see figure 3) consisted of 20 scintillation counters and two Cerenkov counters, the dimensions of which are given in table 1. The configuration at 1300 MeV was essentially the same as shown in figure 3, except that the polyethylene absorber was thicker in order to increase the kaon range. Because this range had to be decreased for the 1100 MeV point, counters 9 and 10 were removed and counter 8 was included in the slowing section. During the kaon runs, particles were required to stop in one of the three thick δR counters (δR1, δR2, δR3). The angular acceptance was defined by the target and by the small aperture counter (12), and the particle energy was adjusted by varying the quantity of polyethylene absorber. Counters 1 to 12 measured the ionization energy loss of slowing particles. The two Cerenkov counters (C1 and C2) with a threshold at $\beta = 0.66$ rejected fast pions and electrons. The two counters (CAL 1 and CAL 2) at the end of the telescope defined protons of fixed range used for the calibration

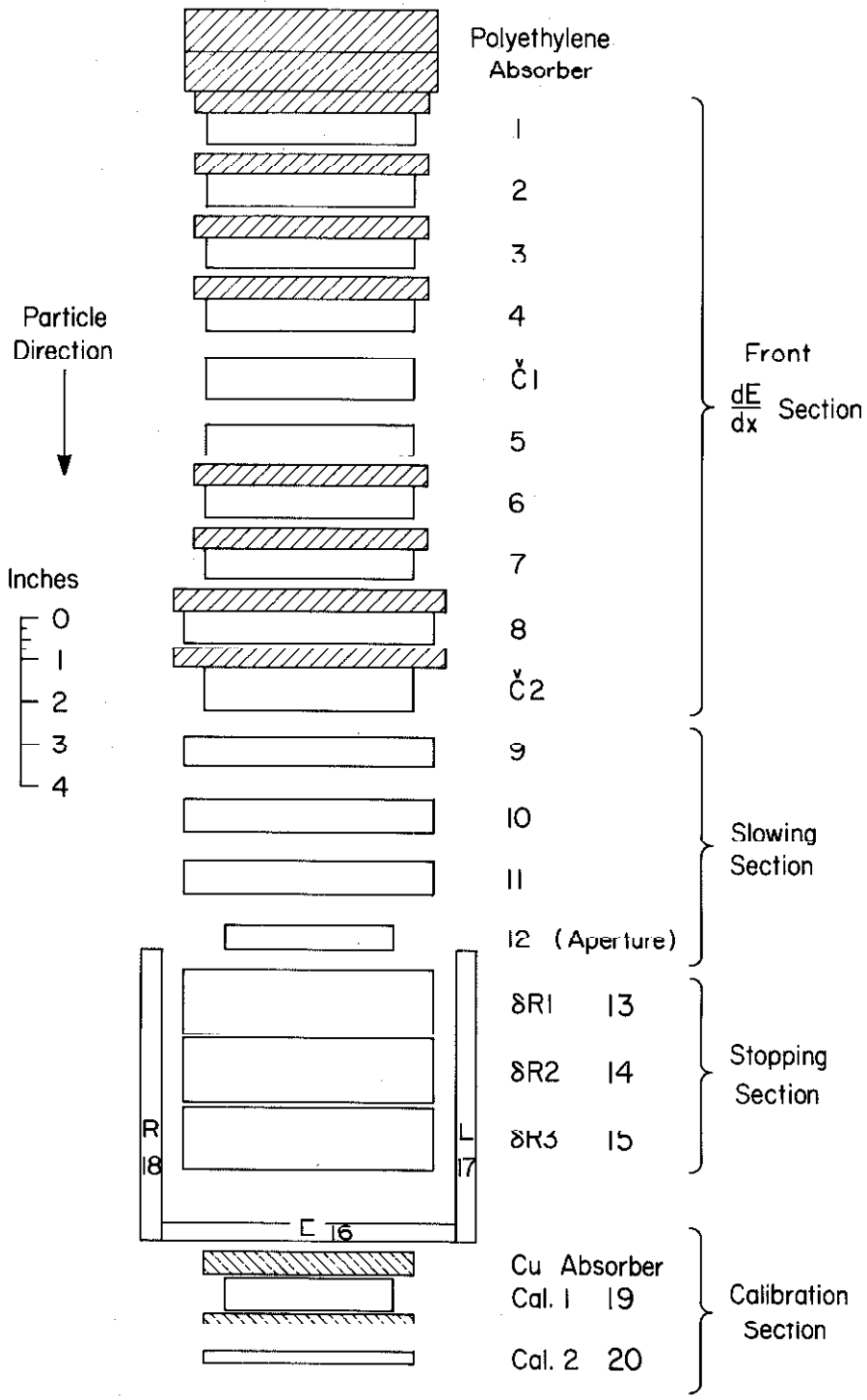

FIGURE 3: K-Telescope Configuration at 1200 MeV

TABLE 1

Counter Data for K-Telescope

Number	Area (inches)	Thickness (inches)	Type	Function
1 - 5	5 × 5	3/4	Scintillator	Front Section - dE/dx
6 - 7	5 × 6	3/4	Scintillator	Front Section - dE/dx
8 - 9	6 × 6	3/4	Scintillator	Front Section - dE/dx
10 - 11	6 × 6	3/4	Scintillator	Slowing Section
12	4 × 5	3/4	Scintillator	Slowing Section - Aperture
13 - 15	6 × 7	1-1/2	Scintillator	Stopping Section
16	7 × 8	1/2	Scintillator	End Counter
17 - 18	8 × 7	1/2	Scintillator	Side Counters
C1 - C2	5 × 6	1	Cerenkov $\beta > 0.66$	Veto Fast Pions
19	5 × 4	3/4	Scintillator	Calibration
20	7 × 5	1/4	Scintillator	Calibration

TABLE 2

Counter Data for Λ-Telescope

Number	Area (inches)	Thickness (inches)	Type
1A - 1B	5-1/2 × 7	1/2	Scintillator
2A - 2B	6 × 7-1/2	1/2	Scintillator
CA - CB	6 × 7-1/2	1	Cerenkov (β>0.66)

of the other scintillators in the K-telescope. The side counters (L and R) detected kaon decay particles as a check on the particle identification, but were not required during the final runs. When the side counters were not used, the efficiency of the K-telescope for kaons was about 30% (see section 5.3).

On the other side of the photon beam, above and below the plane of production, were the two Λ-telescopes, which detected the decay proton from the associated Λ-hyperon. The difference of the counting rates of these two Λ-telescopes was dependent on the Λ polarization.[14] Each Λ-telescope contained two scintillation counters and a Cerenkov counter, the sizes of which are shown in table 2. The absorber was chosen so that the least energetic decay proton would travel through both scintillators. The most energetic decay protons were below the threshold of the Cerenkov counter, which rejected fast pions. In order to reduce counting rates from low energy electrons in these large area telescopes at forward angles, the counters had to be surrounded by several inches of parafin or polyethylene. Because of showers, lead usually increased the electron background.

The combined efficiency of the two Λ-telescopes was about 45% for decay protons, and, since the Λ decayed into a proton 67% of the time, the total efficiency of the Λ-telescopes was 30%.*

* The Λ-telescopes, which were sensitive only to particles at forward angles, did not detect most of the π^-'s associated with the Λ decay, because, unlike the protons, the π^-'s were not concentrated toward forward angles. Also, the Cerenkov counter vetoed about 50% of the π^-'s. (See section 5.3.1).

Although the original function of the Λ-telescopes was only the measurement of the polarization, the high background from nuclear interactions in the K-telescope made the detection of a Λ decay an essential step in identifying kaons unambiguously. As a result, a total kaon detection efficiency of about 9% was obtained.

2.3 Electronics

The light outputs from all counters were converted to electrical pulses by RCA 6810A photomultiplier tubes and processed by the electronic circuits shown in the simplified block diagram of figure 4. For those events electronically preselected as resembling kaons, the pulse-heights from scintillation counters 1 to 18 of the K-telescope were recorded. The preselection occurred in two time ranges - namely, a fast preselection with resolving times of the order of 5 ns and a slow preselection operating between 50 ns and 300 ns.

Basically the function of the electronic preselection was to reduce the counting rates to a level where the data could be handled by a digital computer. For example, typically 2×10^6 particles entered the K-telescope for each detected kaon. The fast preselection reduced this rate to 1.5×10^4, while requiring a coincidence with either Λ-telescope further reduced the rate to 150 events per detected kaon. The slow preselection passed about 20 events per detected kaon to the computer for final analysis.

As a part of the fast preselection, a 4 ns coincidence circuit selected those particles passing through the front and aperture counters (1 and 12) of the K-telescope, but not triggering either

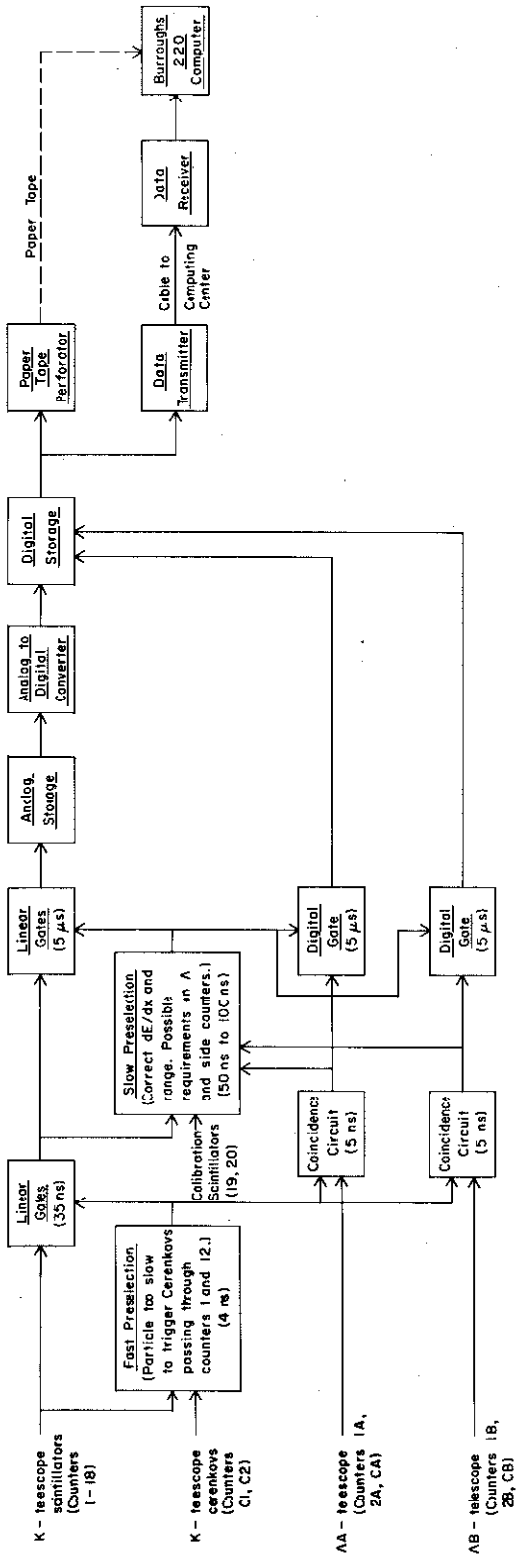

FIGURE 4: Simplified Electronic Block Diagram

K-telescope Cerenkov counter. For such an event, 35 ns linear gates were opened, and the outputs of the eighteen scintillators of the K-telescope were passed to the slow preselection and to the pulse-height analyzer. In addition, a pair of 5 ns coincidence circuits determined if either Λ-telescope detected a coincident particle passing through both scintillators (1A and 2A or 1B and 2B), but not triggering the corresponding Cerenkov counter (CA or CB). Such an event was potentially a kaon with detected Λ decay proton, although, because of the high rates in the Λ-telescopes, most such coincidences were actually accidentals.

The slow preselection contained amplitude windows on the front eight scintillators of the K-telescope and defined the particle range by requiring a coincident pulse in δR1 (13) and no pulse in the end counter (16). The particle to be accepted here had to have a kaon-like rate of energy loss (dE/dx) in the first eight counters and must have stopped between the front of δR1 and the end of δR3. Also, the presence of a coincident Λ-telescope particle could be required for the slow preselection to accept the event. Pulses in the side counters (17 and 18) or in the calibrate counters (19 and 20) could be similarly used.

When the slow preselection accepted an event, 5 μs linear gates in the pulse-height recording system [15] were opened and passed the outputs of the 18 fast gates. The output pulses from the 5 μs gates were stored on capacitors, the voltage on which was scanned sequentially by an analog-to-digital converter. The result of the analog-to-digital conversion was placed in a digital storage,

which also recorded if a coincident particle had been detected by either Λ-telescope. The content of the digital storage was either recorded by a paper tape perforator or transmitted directly to a digital computer.[16]

2.4 Data Analysis

The pulse-height data were then processed by a digital computer. Because only the relatively slow Burroughs 220 computer was initially available at Caltech, computer time had to be carefully conserved. The analysis, therefore, contained several stages of increasingly complex computation, so that most background events could be rapidly rejected without resorting to time-consuming, sophisticated calculations. Later when an IBM 7094 computer was installed, the results of the Burroughs 220 analysis programs were further processed. These programs were nearly all written by Donald Groom, and their details can be found in his Ph.D. thesis.[14]

Using the Burroughs 220, the data from the pulse-height analyzer were first unpacked and prepared for analysis by the KERN Program,[17] which also checked the data format in order to find errors in the electronics. KERN was the governor program for the rest of the data analysis and controlled which analysis subprogram was to be applied to which events.

The data were then scanned rapidly for easily detected characteristics such as pulse-heights so large as to saturate the pulse-height analyzer, pulse-heights outside computer-set bias windows, or undesired pulses in the end counter. About 70% of the

events were rejected at this stage.

The presence of Λ-telescope and side counter signals were also recorded. By selecting those events showing both a Λ-telescope coincidence and a side counter pulse presumably from a kaon decay particle, a relatively pure sample of kaons could be obtained for checking the effects of the data analysis procedures on kaons. The effect on background events was determined by analyzing events produced when the synchrotron end-point energy was below the kaon kinematical threshold.

The analysis of the remaining events was complicated by two effects. First, the kaons decayed, and the decay particle added unknown amounts to the pulse-heights from the stopping section. (If the decay particle entered the end counter (16) or counters 11 and 12, the event was considered lost, and the counting rates were corrected accordingly.) Second, most background events remaining at this stage were interacting protons, which did not have a unique behavior conducive to a simple statistical test. In order to reject such events, the tests applied to the kaons had to be sufficiently precise, so that the probability of background events appearing kaon-like was small enough for an accurate correction to be made.

In order to test if a particle was a kaon, the range within the stopping section had to be determined. Because this range depended almost exclusively on the counters near the region where the particle stopped, and because the decay particle could be ignored in the front of the telescope, the data from the front and rear of the telescope were handled differently. The point of division was somewhat

arbitrarily chosen so that the front section consisted of eight scintillation counters, while the rear slowing and stopping section contained the remaining seven counters [13]. (For the 1100 MeV point, the front section had seven counters and the rear section six.) The rear section was used to determine the range including decay particle effects. Because the kaons behaved predictably in the front section once the range was determined, a simple χ^2 test could be applied there.

The particle was first assumed to have stopped in the last δR counter having a non-zero pulse-height. The expected pulse-heights in the front section for this case were compared by a χ^2 calculation with the measured values. The approximately 8% of the total number of events having a χ^2 greater than 40 were rejected. (Because seven or eight counters were used in this fit, the most probable value for χ^2 was about 6, so that a negligible number of kaons were lost as a result of this selection.)

A detailed calculation of the range was then made using only the data from the rear section. The following procedure selected the best hypothesis for the effect of the decay particle. An upper limit for the range was obtained by assuming that no decay particle was included in the rear section pulse-heights because the kaon decayed after the fast gates had closed. A lower limit was set by assuming that the pulse-height contribution from a singly charged decay particle in the last counter having a non-zero pulse-height was as large as possible. The range was then computed from this counter alone after subtracting this maximal decay contribution.

Weighted averages of ranges computed for counters the slowing particle traversed formed more reasonable intermediate values. The following statistical parameter U_j was computed for each range R_j:

$$U_j = \frac{1}{N(0.1)^2}\left[\sum_{\substack{\text{slowing}\\ \text{section}}}\left(\frac{L_i - L_{ij}}{L_{ij}}\right)^2 + \sum_{\substack{\text{stopping}\\ \text{section}}}\begin{cases}\left(\dfrac{L_i - L_{ij}}{L_{ij}}\right)^2 & \text{if } L_i < L_{ij} \\ 0 & \text{if } L_i > L_{ij}\end{cases}\right] \qquad (2)$$

where: L_i = Pulse-height in the i^{th} counter.

L_{ij} = Calculated pulse-height in the i^{th} counter assuming that the range was R_j and that the particle was a kaon.

N = Number of counters showing pulses.

Large pulses were admitted with no penalty in the stopping section so as not to discriminate against kaon events where the decay particle signals added to the stopping section pulse-heights. Events with pulse-heights consistently below those expected for normally stopping kaons were penalized to reject fast protons scattering out of the telescope without passing through the end counter. The smallest of the U_j was chosen to indicate the best hypothesis for the range and was used as the parameter U in further calculations.

Figure 5a shows a typical distribution of U for 1473 events selected to be kaon-like in the front section. Figure 5b shows the distribution of U for 1665 simulated kaon events generated by a Monte

Carlo program. For $U < 1.5$ the distributions for simulated kaons and real kaons were nearly identical. However, the real data showed a long, flat tail which persisted below the kinematical threshold for kaon production. If a side counter pulse were required, this tail nearly disappeared. As a result, the events with $U > 2.0$ were interpreted as background and were rejected. This bias eliminated about 15% of the total events and, based on the events showing side counter pulses and on the Monte Carlo analysis, resulted in a $2.6 \pm 2.3\%$ loss of kaons.

Using the range determined above, a parameter S was computed for the front section as follows:

$$S = \frac{1}{(0.1)^2} \sum_{\substack{\text{Front} \\ \text{Section}}} \left(\frac{L_i - L_{io}}{L_{io}} \right)^2 \qquad (3)$$

where: L_i = Pulse-height in the i^{th} counter.

L_{io} = Expected pulse-height in the i^{th} counter using the range giving the minimum U_j assuming that the particle was a kaon (or proton).

Figure 6 shows distributions for S for kaon-like events, kaon events showing a side-counter pulse, and for stopping protons. (The analysis program could be easily instructed to use values of L_{io} calculated assuming that the particle was a proton instead of a kaon. The proton fit was made in this way.) Only about 1% of the events analyzed by the computer were eliminated by requiring that S be less than 25. The values of U and S for the remaining 5 to 10% of the total events

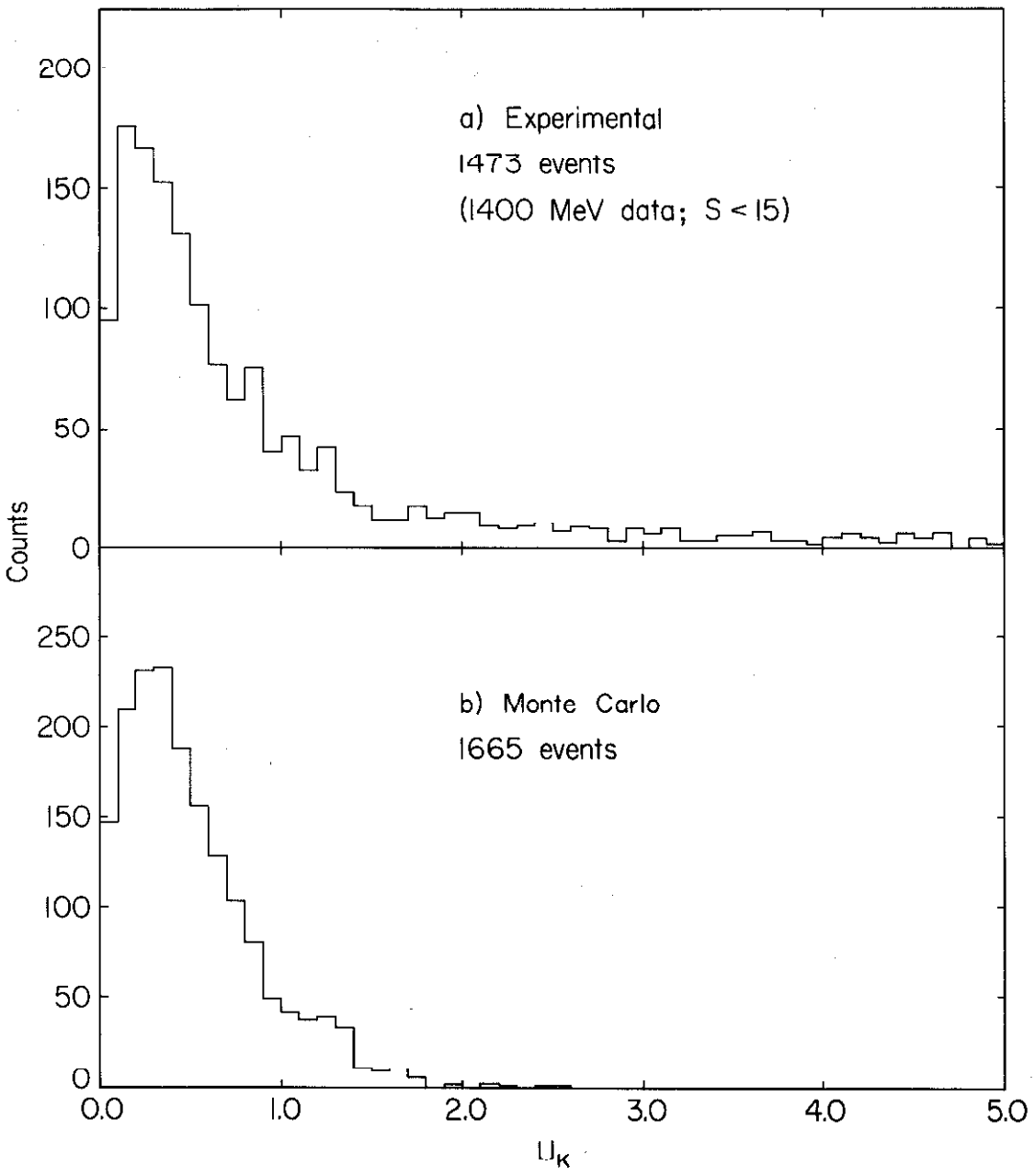

FIGURE 5: Distributions for U

were then printed out. These events were a mixture of kaons with 2 to 25% background.

The distribution in S of the background was determined by lowering the synchrotron end-point energy below the kinematical threshold for kaon production, and analyzing the resulting events. This distribution was found to rise linearly from zero to S = 10 and then remain constant to beyond S = 25.

The distribution for kaons could be estimated from known χ^2 distributions. If the counter response were normal with 10% resolution, then the S distribution would be a χ^2 distribution with as many degrees of freedom as there were counters in the front section. Because the counter pulse-height distribution was slightly skewed [45], the S distribution would be expected to be more skew than the corresponding χ^2 distribution.

Using the IBM 7094 computer, a maximum-likelihood fit was made to the S spectra using the above background distribution and a χ^2 distribution of varying number of degrees of freedom for the kaon events. The parameters used in the fit were the relative amount of background (b) and the relative width of the counter resolution (r).

The optimum number of degrees of freedom for the χ^2 distribution was found to lie between the number of counters in the front section and one less than this number. Because lowering the number of degrees of freedom of a χ^2 distribution increases its relative width, the tendency of the optimum number of degrees of freedom to be less than the number of counters in the front section was interpreted as resulting from the skewness of the counter

pulse-height distributions. The background corrections for these two cases were averaged for the cross-section measurement. The dotted curves in figure 6 represent the results of this fitting procedure.

The number of kaons lost by truncation at S = 25 was calculated from the χ^2 distributions and was found to be less than 1%. Because this efficiency was so large and was also insensitive to the parameters of the fit,[14] a negligible error was produced by the truncation. The usual counting statistics resulted in an error equal to the square root of the number of events with $S \lesssim 25$. Further statistical errors resulted from uncertainties in the value of b, arising both from the fitting at a fixed number of degrees of freedom and from the choice of the appropriate number of degrees of freedom. The error in the background b resulted in a statistical error in the cross-section of typically ± 5%.

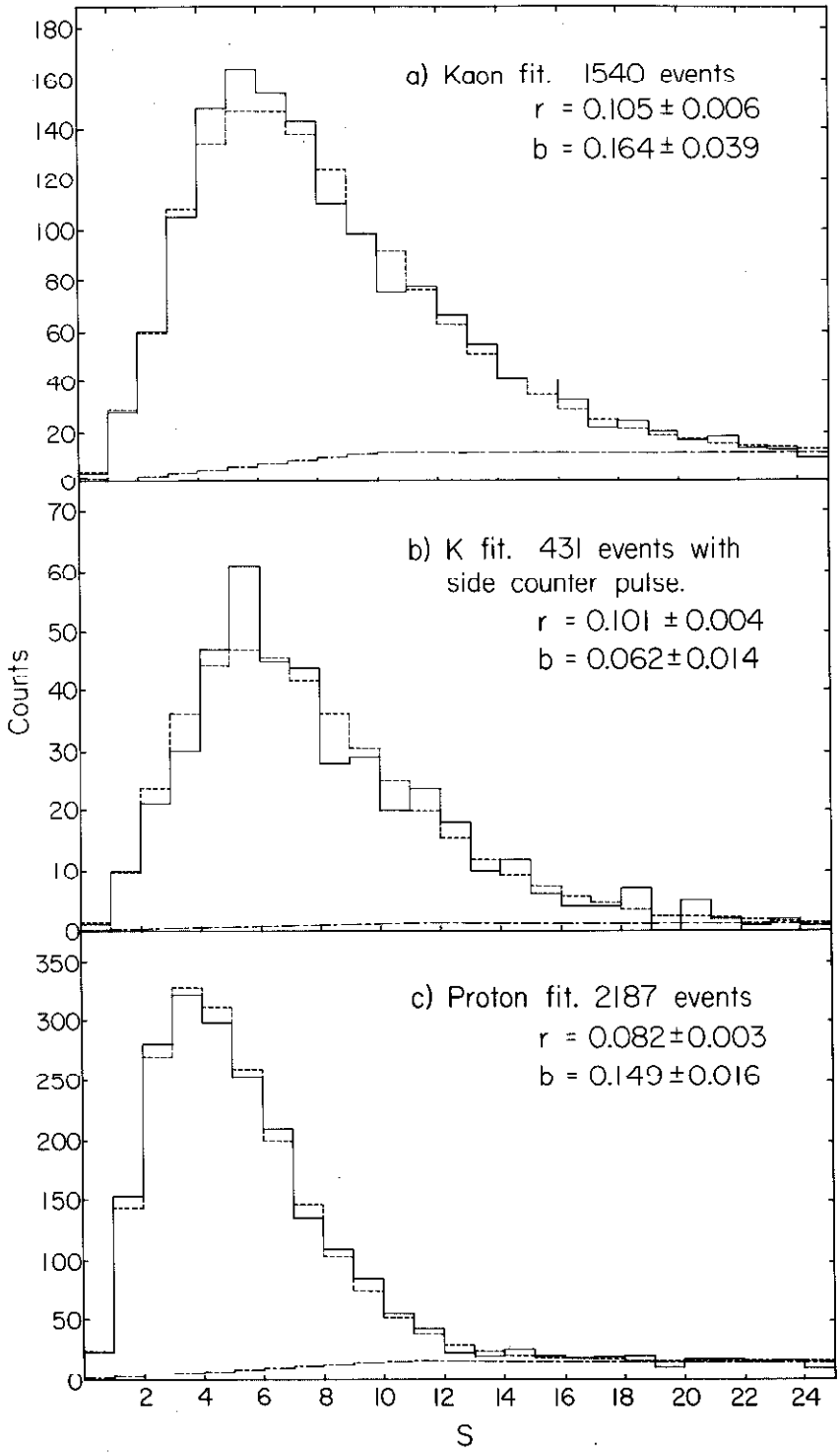

FIGURE 6: Distributions for S

3.0 ELECTRONIC INSTRUMENTATION

3.1 General

Because my principal contribution to this experiment was the development of the electronic instrumentation, it will be described here in detail. In the design of a system to perform the tasks outlined in the previous section, three general difficulties had to be overcome. First, because low energy electrons associated with the photon beam produced average counting rates from 10^5 to 5×10^6 pulses per second in the front scintillation and Cerenkov counters, fast coincidence and gating circuits had to be used to minimize accidental coincidences or anti-coincidences, and the number of such accidental counts had to be measured. Accidental effects produced a correction of about 15% to the cross-section.

Second, since the rate of kaons with detected Λ decay was about ten per hour, runs lasting ten hours were usual. In order to make such long runs reliably with an electronic system containing 3000 active elements, the mean time to failure of each active element had to exceed 100,000 hours. Thus, with the exception of the high voltage power supply, conservatively designed solid-state circuitry was used exclusively. Monitoring and testing circuits were also provided to insure proper operation.

Third, because the particle identification was already difficult enough with 10% statistical fluctuations, further widening of these distributions by electronic drifts or resolution was avoided by providing a 2% to 4% stability and resolution for the bias setting and pulse-height analysis.

The electronics used elements of a modular, transistorized instrumentation system,[18] which has been used here[20] and at the Fermi Institute of the University of Chicago.[19] A set of standard circuits, consisting of several types of fully interchangeable units, comprised the logical building blocks of an analog-digital system, which could be adapted to suit the requirements of a particular experiment. The basic units were built on 4.5" × 8.25" epoxy glass printed-circuit boards. The controls and the monitor coaxial connectors were mounted on 1.35" × 5.2" photo-engraved front panels, and the power and the twelve standard signal connections were made via rear 22 pin printed-circuit connectors. Twelve of these boards plugged into a 4.75" × 17" card file equipped with 24 receptacles to accommodate twelve boards and twelve capacitive shields. The signals were carried by short leads to 144 BNC connectors in the rear, and thence to other circuits by terminated 125 ohm coaxial cables.

In addition to the elements of the general purpose instrumentation system, commercial equipment* and circuits constructed on copper modules and in conventional rack mounted chassis were also used. The copper modular construction technique, developed before printed-circuits were adapted to high speed pulse applications, is now considered obsolescent.

A brief summary of the characteristics of most of the circuits used here is given in Appendix B and in reference 18.

* Most of this equipment was purchased from Ransom Research, a Division of Wyle Laboratories, in San Pedro, California.

3.2 Fast Preselection

A block diagram of the fast preselection is shown in figure 7. After amplification by a factor of 10 by a distributed amplifier, the signals from counters 1, 12, C1 and C2 entered the 4 ns K coincidence-anticoincidence circuit. This circuit produced an output signal for a coincident pulse in counters 1 and 12 without a coincident pulse in either Cerenkov counter.

The coincidence circuit signal triggered a discriminator, the output from which passed through the fast gate inhibit circuit and opened the fast gates, when the pulse-height analyzer input gate was not simultaneously open. The fast gate inhibit circuit blocked the fast gate pulse while the analyzer input gate was open. Separate scalers* counted discriminator output pulses and those pulses blocked by the fast gate inhibit circuit. After being delayed so as to be coincident with the middle of the 40 ns discriminator pulse, the signals from counters 1 to 18 were gated by the fast gates. An additional fast gate circuit with grounded input provided a reference zero level.

The output pulse from the K coincidence circuit was also used with the Λ counter signals to define the coincidence between a Λ decay proton and the associated kaon. Because counting rates in excess of 10^6 pulses per second were present in all the Λ counters, the last five dynodes of their phototubes were stabilized by emitter followers [21] to prevent excessive charging of the dynode by-pass capacitors. Also the phototube signals were clipped by 3 ns, 125 ohm

* The scalers, which were manufactured by Ransom Research, had a pulse pair resolution of 1 μs.

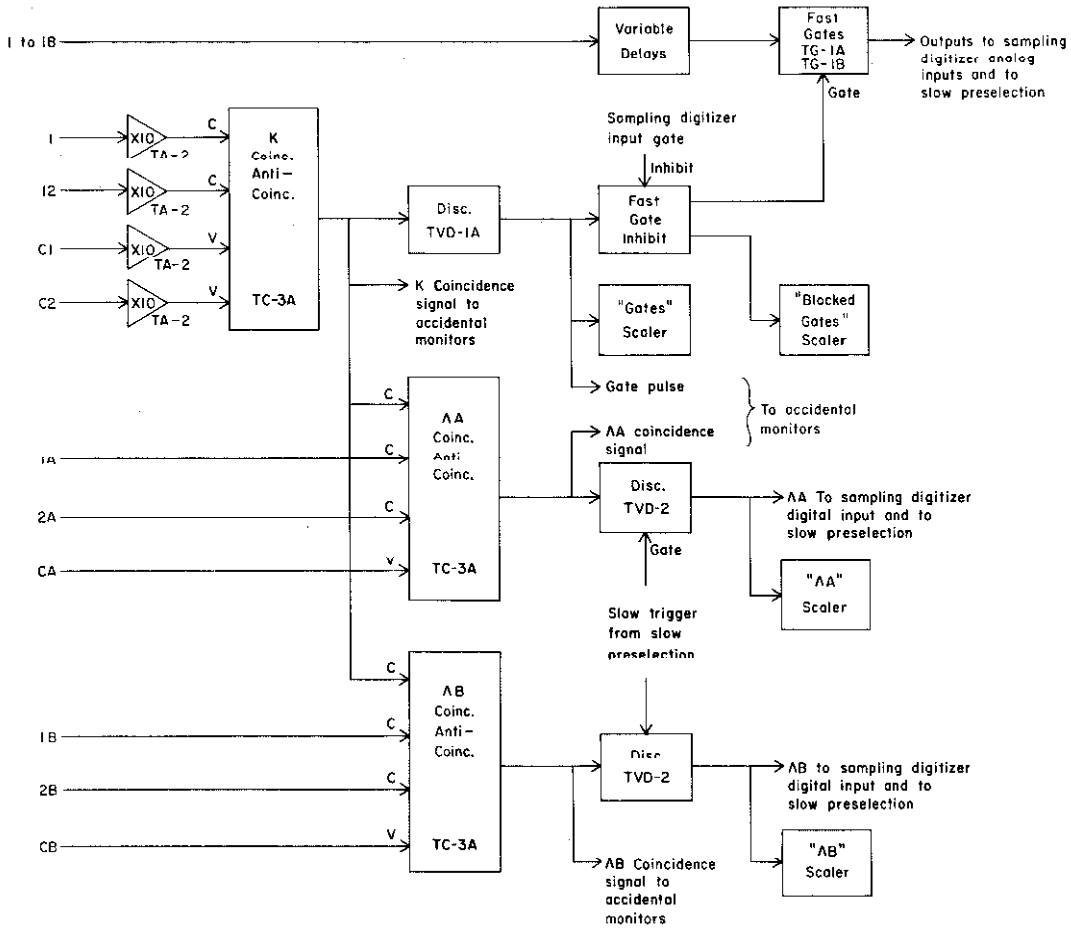

FIGURE 7: Block Diagram - Fast Preselection

cables terminated in 24 ohms to reduce the pulse widths. Coincident pulses from 1A, 2A and the K telescope without a coincident pulse from CA were required for the ΛA coincidence circuit to trigger a discriminator, that could be gated by the output of the slow preselection. The discriminator output was recorded with the pulse-height data and counted by a scaler. The signals from counters 1B, 2B, and CB were handled in the same manner.

3.3 Slow Preselection

A block diagram of the slow preselection is shown in figure 8. After being attenuated by 10 db, the output pulses of the fast gates for counters 1 to 8 were separately added to 10% of the total of counters 13 to 15. The resulting signals were processed by a multifold coincidence-anticoincidence circuit (TC-2),[22] where amplitude windows were set for the first eight counters of the K-telescope. In this circuit, the input signals were first shaped to a 50 ns critically damped pulse and then amplified. The amplified signal was applied to two parallel discriminators, which drove 50 ns coincidence-anticoincidence circuits.

The feedback from the stopping section (counters 13 to 15) was originally intended to permit more stringent selection of kaon-like events by the slow preselection (see Appendix A). However, requiring a coincident Λ event sufficiently reduced the trigger rate, so that biases could be set 35% on either side of the expected kaon dE/dx, and the feedback was no longer necessary to preserve the kaon efficiency.

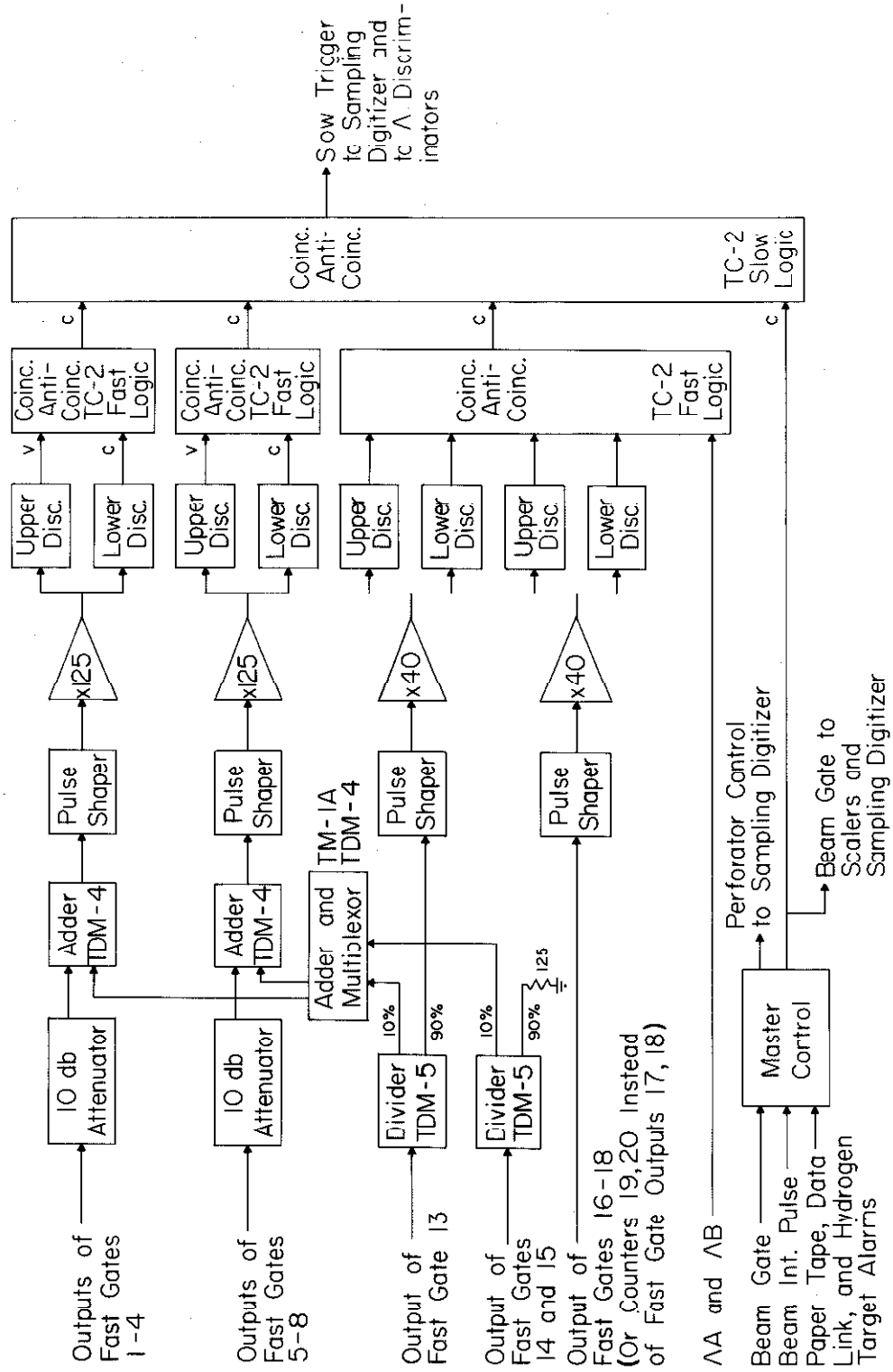

FIGURE 8: Block Diagram - Slow Preselection

The signals from the fast gates for counters 13 (δR1), 16 (End), and 17-18 (Side) or 19-20 (Calibrate) were shaped, amplified, discriminated, and used to drive 50 ns logic circuits, where they could be combined with the ΛA and ΛB signals, which indicated if a Λ decay proton was detected. The outputs of these logic circuits were then combined with the outputs of the 50 ns coincidence circuits for counters 1 to 8 by a 300 ns coincidence-anticoincidence circuit, which generated the slow trigger. By the proper setting of switches, several conditions could be imposed on the signals 13, 16, 17, 18, 19, 20, ΛA, and ΛB for a slow trigger to be produced. For example, with 13 in coincidence and 16 in veto, a particle had to stop between counters 13 and 16. Also, a slow trigger could indicate the detection of a coincident particle by one of the Λ-telescopes or calibrate counter pulses lying within amplitude windows.

The 300 ns coincidence circuit, scalers, and the pulse-height analyzer were gated by a beam gate, which was "on" when a photon beam was being produced. This gating prevented about 80% of the spurious triggers resulting from noise or background radiation. The beam gate, and thus the experiment, were controlled by the Master Control, [23] which also activated the motor of the paper tape perforator. By counting beam integrator pulses (from the synchrotron control circuits), the Master Control monitored the amount of integrated beam intensity during a particular run, and could be made to stop the run at the end of a preset amount of total beam. Also alarm signals from the liquid hydrogen target, the paper tape perforator, or the computer data link could stop the experiment.

3.4 Pulse-Height Analysis

The pulse-height analysis was performed by the Sampling Digitizer,* which could sort the amplitudes from as many as 25 simultaneous input signals into 100 channels each. The outputs of the fast gates for counters 1 to 18 entered the pulse-height (analog) inputs together with the output of the zero reference gate. The Sampling Digitizer also could accept digital signals, the presence or absence of which at the time of triggering was recorded. The outputs of the Λ-telescope discriminators (ΛA and ΛB) entered two of these digital inputs. The output of the Sampling Digitizer was either recorded on perforated paper tape or directly transmitted to the computer by a data link. (16)

A functional block diagram of the Sampling Digitizer is shown in figure 9. The sequence of operations was determined by the Control, which consisted of digital logic circuits, the operation of which was synchronized to a crystal controlled oscillator. Clock pulses derived from this oscillator were counted to generate all critical timing signals. Although the Control was rather complex, it contained only standard digital techniques, and its internal operation will not be discussed here in further detail.

The overall operation of the instrument was controlled by the beam gate. Only when the beam gate was open could the Sampling

* This instrument was constructed in collaboration with Ransom Research, a Division of Wyle Laboratories, of San Pedro, California. Full details of its operation can be found in the Instruction Manual, Model 1138B, Sampling Digitizer, and Addenda and Errata to the Instruction Manual, Model 1138B, Sampling Digitizer. In addition, a condensed description can be found in reference 15.

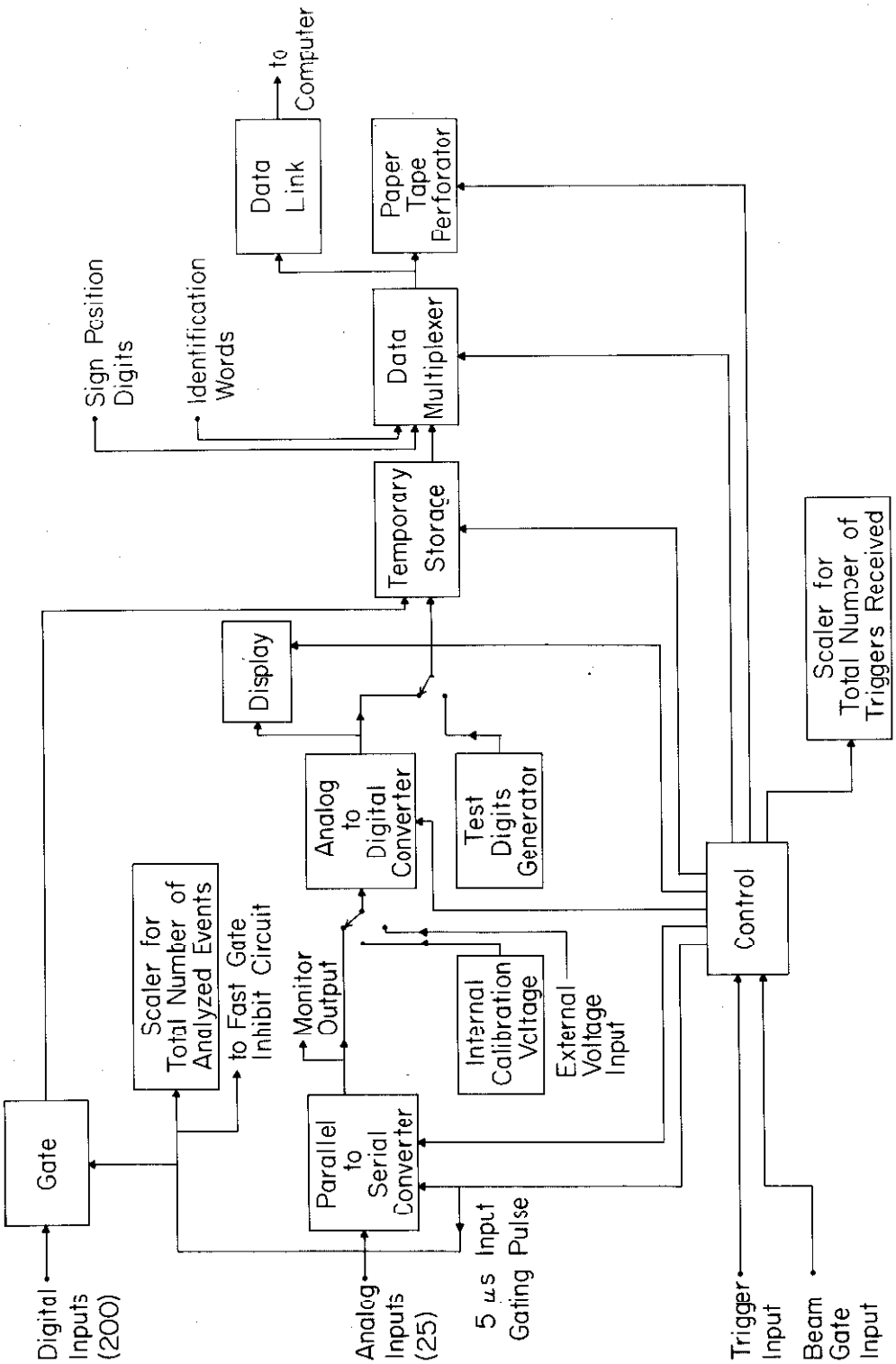

FIGURE 9: Block Diagram - Sampling Digitizer

Digitizer accept events, consisting of input signals in coincidence with a trigger pulse. After the arrival of an accepted trigger pulse, the input gates at each analog input were opened for 5 μs. Pulses which appeared at the analog inputs during this period were accepted and stored by the parallel-to-serial converter. The stored analog information was then presented at the output of this converter as a sequence of twenty-five 320-μs wide pulses, the amplitudes of which were proportional to the input pulse-heights. These pulses were fed to the input of an analog-to-digital converter which generated a binary-coded, two-digit decimal number for each successive input pulse. These numbers, together with the gated digital inputs, were recorded in a 200 binary bit temporary storage. The parallel-to-serial converter was then reset in preparation for another trigger. The analysis and reset cycle described above required about 15 ms when all 25 analog inputs were used.

When paper tape was the output medium and after an event had been recorded in the temporary storage, the closing of the beam gate initiated the readout sequence. Then the data multiplexer scanned the information in the temporary storage, the sign digits which were determined by preset front panel switches, and the end-of-word character, which was the number 13 generated by internal dc voltages. These digits were combined to produce standard Burroughs 220 computer words, which began with a sign digit, then contained ten decimal digits from the temporary storage, and ended with an end-of-word character. The output of the data

multiplexer controlled the operation of a paper tape perforator,* which was capable of operating at 72 characters per second. The capacity of the temporary storage was five words, which required 845 ms to read out. If the entire capacity of the temporary storage was not used, time and paper tape could be saved by setting the readout to operate on only those words used. Because the synchrotron was pulsed each 1.05 s, about 200 ms were available during each pulse for collecting data. The maximum time during which the synchrotron produced a photon beam was about 100 ms.

When the data link was being used, the readout sequence began immediately after the completion of the analog-to-digital conversion of the first input. The output of the data multiplexer was then transmitted directly to the computer memory at a rate of 1280 characters per second.** In this mode of operation the instrument deadtime was 50 ms.

In an alternative mode of operation, the data multiplexer scanned digits which had been set up on front panel switches rather than those in the temporary storage. These preset digits served as identification words on the tape.

The number of analyzed events and the number of triggers passed by the beam gate were counted by decimal scalers. The difference of these counts was the number of events lost during the

---

* The perforator was a special modification of the Model 420 PR manufactured by the Tally Register Corporation of Seattle, Washington.

** If the Sampling Digitizer were used with an IBM 7090 Computer, data could be transmitted at a rate of 6400 characters per second, reducing the dead time to about 17 ms.

instrument dead time.

3.5 Accidental Monitoring

Because accidental effects resulted in a 15% correction to the cross section, accidental monitoring by the circuits shown in figure 10 was required. The basic operation of the three systems which measured the probability that an event was lost because of an accidental pulse from one of the Cerenkov counters is summarized by figure 11. If the primary coincidence circuit had a veto resolving time of τ_1, the number of events accidentally vetoed (N_A) would be:

$$N_A = \int_0^T R_V R_C \tau_1 \, dt \qquad (4)$$

where: R_V = rate of veto pulses.

R_C = output rate of primary coincidence circuit.

T = time over which the measurement was made.

if: $R_V \tau_1 \ll 1$

If the delay at the input to the accidental monitor coincidence circuit was sufficiently large to prevent it from counting true coincidences, its output rate (R'_A) would be entirely caused by accidental coincidences between the veto signal and the output of the primary coincidence circuit. If the delayed veto rate (R'_V) and the accidental monitor resolving time (τ_2) were sufficiently small so $R'_V \tau_2 \ll 1$, then the output rate (R'_A) from the accidental monitor would be given by:

$$R'_A = R'_V R_C \tau_2 \qquad (5)$$

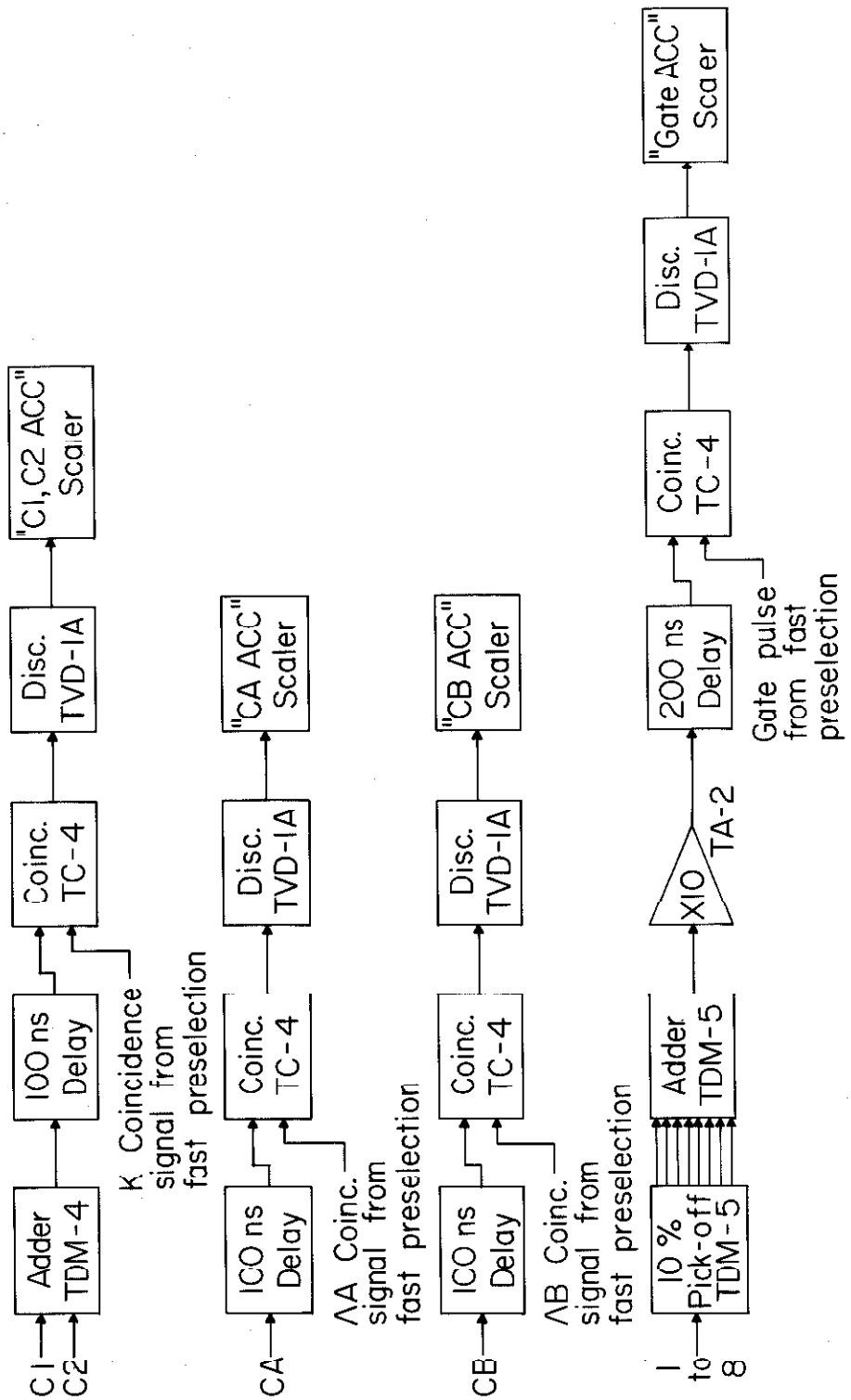

FIGURE 10: Block Diagram - Accidental Monitor

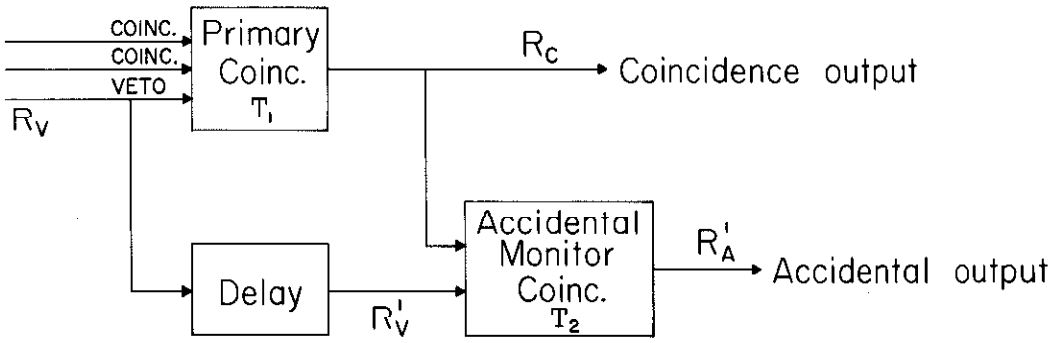

FIGURE 11: Accidental Monitoring Scheme

and the total number of counts (N'_A) from the accidental monitor would become:

$$N'_A = \int_o^T R'_A \, dt = \int_o^T R'_V R_C \tau_2 \, dt \tag{6}$$

If the delay was equal to the time required for an electron bunch* to travel an integral number of times around the synchrotron, then:

$$R'_V = R_V \tag{7}$$

and

$$N'_A \cong \frac{\tau_2}{\tau_1} N_A \tag{8}$$

and the coincidence output should be corrected by a factor:

$$1 + \frac{N_A}{N_C} = 1 + \frac{\tau_1 N'_A}{\tau_2 N_C} = 1 + K \frac{N'_A}{N_C}$$

$$K \equiv \tau_1/\tau_2 \tag{9}$$

where N'_A and N_C were recorded by scalers and K was a measured constant given in table 3.

In order to measure the probability that an accidental pulse from one of the K-telescope Cerenkov counters caused a kaon event to be lost, the outputs of C1 and C2 were added, delayed by 100 ns, and placed in 5 ns coincidence with the output of the K-telescope fast coincidence circuit. The output of the accidental coincidence circuit

* The electrons in the synchrotron were bunched at the same phase of the 40 MHz radio frequency system. The time required for a bunch to complete one orbit was 100 ns.

drove the "C1,C2 Accidentals" scaler via a discriminator. The ratio of the number of counts in this scaler to the number of counts recorded by the "Gates" scaler was proportional to the probability that a kaon event was accidentally vetoed by a Cerenkov pulse. In order to ascertain the proportionality constant, the output of the K^+ fast coincidence circuit was delayed by 100 ns so that fast pions formed true coincidences between the K^+ fast coincidence circuit and the accidental coincidence circuit. In this way, the resolving time of the accidental coincidence circuit was measured, and the proportionality constant (K) was taken as the ratio of the veto resolving time of the K^+ fast coincidence circuit to the resolving time of the accidental coincidence circuit. In this case the resolving time was defined as the ratio of the area under the timing curve to the peak value. The probability that a Λ decay proton was lost because of an accidental pulse from CA or CB was measured by a similar technique.

The singles rates from the Λ-telescope coincidence circuits were measured with a 40 MHz scaler and correlated with the average number of beam gates between BIPS. The coincidence circuit dead time was then checked by placing the Λ telescopes in front of the K telescope and measuring the efficiency of the Λ-telescopes for protons detected by the K-telescope. All deviations from 100% efficiency were attributed to coincidence circuit dead time, which was measured in this way to be 16 ns. Also, the outputs of the coincidence circuit limiters were observed directly with an oscilloscope (Tektronix 581) and found to last for 14 ns to 18 ns depending on the input pulse

TABLE 3

Accidental Monitor Proportionality Constants

Accidental Scaler	Normalizing Scaler	K	Percentage Error in K	Remarks
C1, C2 Acc.	Gates	1.0	± 30%	Included in gate accidentals
CA Acc.	ΛA	1.2	± 20%	
CB Acc.	ΛB	0.95	± 20%	
Gate Acc.	Gates	0.37	± 20%	
Blocked Gates	Gates	1.0	± 2%	
Blocked Gates	Sampling Digitizer Analyzed Events	0.2	± 5%	
Gate Acc.	Gates	0.08	± 30%	K^+ Coinc. Dead Time
Sampling Digitizer Triggers-Analyzed Events	Triggers	1.0	< 1%	
Bips	Beam Gates	0.32	± 40%	ΛA Coinc. Dead Time
Bips	Beam Gates	0.30	± 40%	ΛB Coinc. Dead Time

$$K = \frac{\text{Fraction of Kaons Lost}}{\text{Accidental Scaler Counts/Normalizing Scaler Counts}}$$

height. The proportionality constant (see table 3) between beam intensity and the fractional coincidence circuit dead time was derived from a dead time of 16 ns per pulse and the measured singles rate of 2×10^6 pulses/second at ten beam gates per BIP.

If an accidental pulse greater than about 1/2 minimum ionizing passed through one of the first eight fast gates together with a kaon signal, the bias windows in the slow preselection would probably reject the event. This type of accidental loss was monitored by adding together 10% of the ungated outputs of counters 1 to 8 and placing them in delayed coincidence with the gate pulse. The proportionality constant (see table 3) in this case was both calculated from the known gate and TC-2 resolving times and measured with random signals from a pulser and Co^{60} source. The two methods agreed within 10%.

Because the threshold of the K^+ fast coincidence circuit was also set at about 1/2 minimum, and because singles-rate measurements showed that 40% of the gate accidental counts came from the first counter, the gate accidental rate could also be used to measure the probability of kaon loss from the K^+ coincidence circuit dead time. Because this correction was small ($\sim$ 0.5%), the dead time resulting from the aperture counter (12), which counted an order of magnitude slower than the front counter (1), was neglected.

The monitoring of the accidental vetos from the K^+-telescope Cerenkov counters was further checked by placing one Cerenkov counter in coincidence with the front aperture counters and setting

the slow preselection to count only protons of insufficient velocity to trigger the Cerenkov counters. (The other Cerenkov counter was disconnected.) Then the only counts which could be recorded would result from an accidental Cerenkov pulse in coincidence with a proton. However, over an order of magnitude fewer proton events were recorded than would be expected from the accidental monitor rate. The most probable explanation was that the Cerenkov counter rate was primarily caused by fast electrons or pions traveling through at least one of the eight front scintillators. Because the fast gate open time was greater than the veto resolving time, the energy loss from such a fast electron or pion would be added to the proton energy loss and cause the pulse-height to lie outside of the window set by the slow preselection. Such an event would be recorded as both a "C1, C2 Accidental" and as a "Gate Accidental." This explanation was further checked by observing the "Gates" rate with the Cerenkov counter in coincidence but delayed by 25 ns. In this case the "Gates" rate equaled the rate predicted by the Cerenkov accidental monitor. Thus, because at least 90% of all accidental vetos by the K^+-telescope Cerenkov counters were also gate accidentals, the "C1, 2 Accidental" correction was ignored.

As discussed in the previous section, the loss of events caused by the Sampling Digitizer dead time was monitored by the analyzed events and triggers scalers. The probability that an event was rejected by the fast gate inhibit circuit was given by the ratio of the counts in the "Blocked Gates" scaler to those in the "Gates" scaler. The probability that the fast gates opened again during the 1 μs delay

before the fast gate inhibit circuit blocked fast gating pulses was approximately 0.2 times the ratio of the number of blocked gates to the number of analyzed events. This type of accidental would probably cause a kaon event to be rejected by the computer, since additional pulses had to be present in at least counters 1 and 12 in order for the gates to be opened a second time.

Because of the stringent requirements set by the data analysis for the acceptance of an event as a kaon, the probability of accidentals in eighteen counters making a non-kaon event look enough like a kaon to be accepted was considered negligibly small. The general magnitude of the various accidental corrections are given in section 5.3.3 and in table 8.

3.6 Power

Regulated DC power was provided by three sets of power supplies - one for the cathode and dynode voltages of the photomultiplier tubes, the second for the Sampling Digitizer, and the third for the remaining transistor electronics. These supplies operated from 116 volts, 60 cycle power, regulated to ± 1%. Isolation transformers prevented ground loop pick-up.

An Alfred Model 233A supply regulated to ± 0.02% generated 2.3 KV, which was distributed to the 26 photomultipliers of the system. The voltage applied to each photomultiplier could be separately adjusted by switchable taps on a chain of ten voltage regulator tubes (OG3). A simultaneously switched resistive load kept the regulator tube current constant as the voltage was switched. The dynode voltages were provided by resistive dividers with condensers to

prevent pulses from changing the dynode voltages. Emitter followers stabilized the last five dynodes of the photomultipliers for the Λ-telescopes.

The Sampling Digitizer had supplies regulated to ± 0.02% for the ± 27V and -6.3V used in the parallel-to-serial converter and for the + 12V used as the reference for the analog-to-digital converter. The digital circuits operated on ± 12V power, regulated to ± 2%.

The remainder of the electronics operated from regulated (± 0.04%) supplies,* which generated ± 27V and -6.3V. These voltages were interlocked so that all voltages would be shut off if any voltage deviated more than ± 20% from the nominal value. Remote sensing minimized the effects of voltage drops from wires carrying up to five amperes. For uncritical applications, such as light bulbs and relays, ± 16 V unregulated power was used.

3.7 Monitoring and Testing

The following monitoring and testing systems were provided to insure proper operation of the experiment. A digital voltmeter** accurate to ± 0.01% measured the critical voltages of the Sampling Digitizer and the outputs of the Lambda power supplies. The photomultiplier cathode voltages were measured by the digital voltmeter using a stable (40 ppm/°C) resistor divider and a current balancing

---

* The power supplies, manufactured by Lambda, are as follows:

+27V, 5A	LA 50-03AM
-27V, 10A	LA 100-03BM
-6.3V, 10A	LE 109M

** Stevens-Evans, Model 910-VR

scheme which did not load the circuit being monitored.

The circuits of the general purpose instrumentation system had 10:1 resistive dividers with an output impedance of 125 ohms located on the front panels. These monitor outputs could be observed on an oscilloscope (usually Tektronix 581) and could be shorted without appreciably affecting the operation of the circuit.

The computer performed several checks on the data. For example, the output of the zero reference gate was subtracted from all the pulse-heights to minimize drifts caused by changing pedestals. The computer recorded if the zero level had shifted more than ± 2 channels and if any of the counter outputs were off scale in the pulse-height analysis.

Several provisions were made for testing the Sampling Digitizer. One test circuit read arbitrary two-digit numbers into the temporary storage in order to test the temporary storage and its readout. The analog-to-digital converter could be tested by applying either an internal or an external calibration voltage to its input. A two-decimal digit display indicated the pulse-height of any analog input selected by a front panel switch. The sequential input to the analog-to-digital converter was accessible on the front panel for monitoring on an oscilloscope. In addition, the data link also had a test circuit which transmitted known digits.

A mercury relay pulser with a ± 0.02% regulated power supply generated a pulse similar in shape to a photomultiplier tube output. The pulser output pulse was divided resistively into 30 pulses, which were independently delayed and attenuated so that

their relative timing and amplitude were the same as for the photomultipliers. A patch panel allowed the phototube outputs to be replaced by the pulser outputs or the pulser outputs to enter the Sampling Digitizer analog inputs directly. The pulser supply voltage could also be monitored by the digital voltmeter.

4.0 TESTS AND CALIBRATIONS

4.1 Fast Preselection Tests

The principal element of the fast preselection was the TC-3A coincidence circuit, the time resolutions for which are illustrated in figure 12. The coincident counting rate for protons selected by the slow preselection is shown as a function of the delay of counter 12. Also figure 12 shows the counting rate for minimum ionizing particles selected by the slow preselection as a function of the delay of C1. which was in veto.

Because the accuracy of the Λ polarization measurement was critically dependent on the efficiencies of the Λ-telescopes, these efficiencies were checked by placing the Λ counters in front of the K-telescope. Protons selected by the slow preselection were passed through both the Λ counters under test and the K-telescope. The ratio of the number of ΛA (or ΛB) pulses in coincidence with the slow trigger (indicating a proton selected by the K-telescope) to the number of slow triggers gave the efficiency of ΛA (or ΛB). This technique was also used to set the photomultiplier gains and the timing for the Λ-telescopes. A typical timing curve showing the efficiency of ΛB versus the delay of 2B is shown in figure 13. Deviations from 100% efficiency were consistent with known counting rates and coincident circuit dead times.

Another source of inefficiency for detecting kaons was a possible non-zero probability that the Cerenkov counters detected kaons. This probability was measured for the velocities expected for kaons in the Cerenkov counters using protons selected by the slow

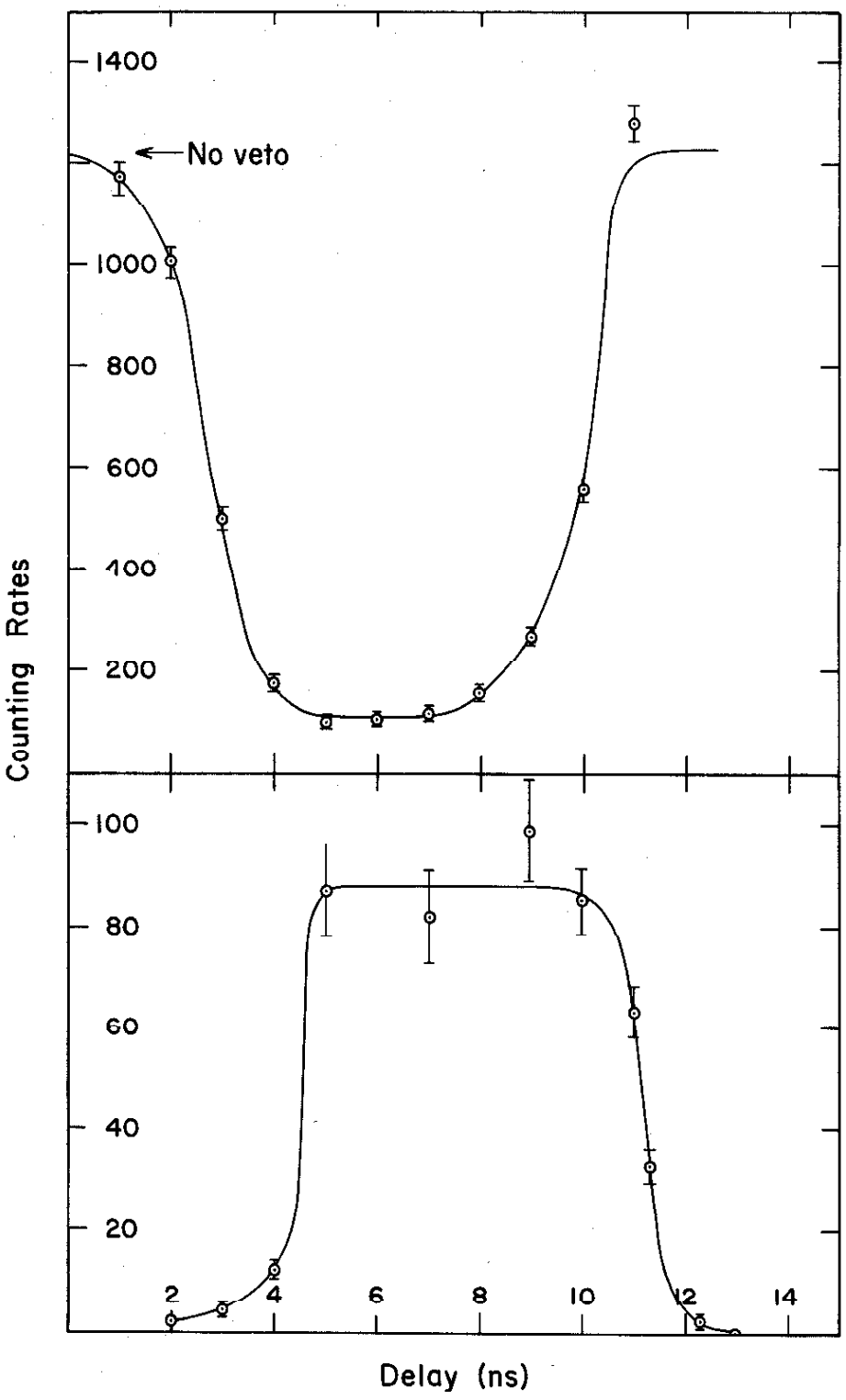

FIGURE 12: Time Resolution of the Fast Coincidence

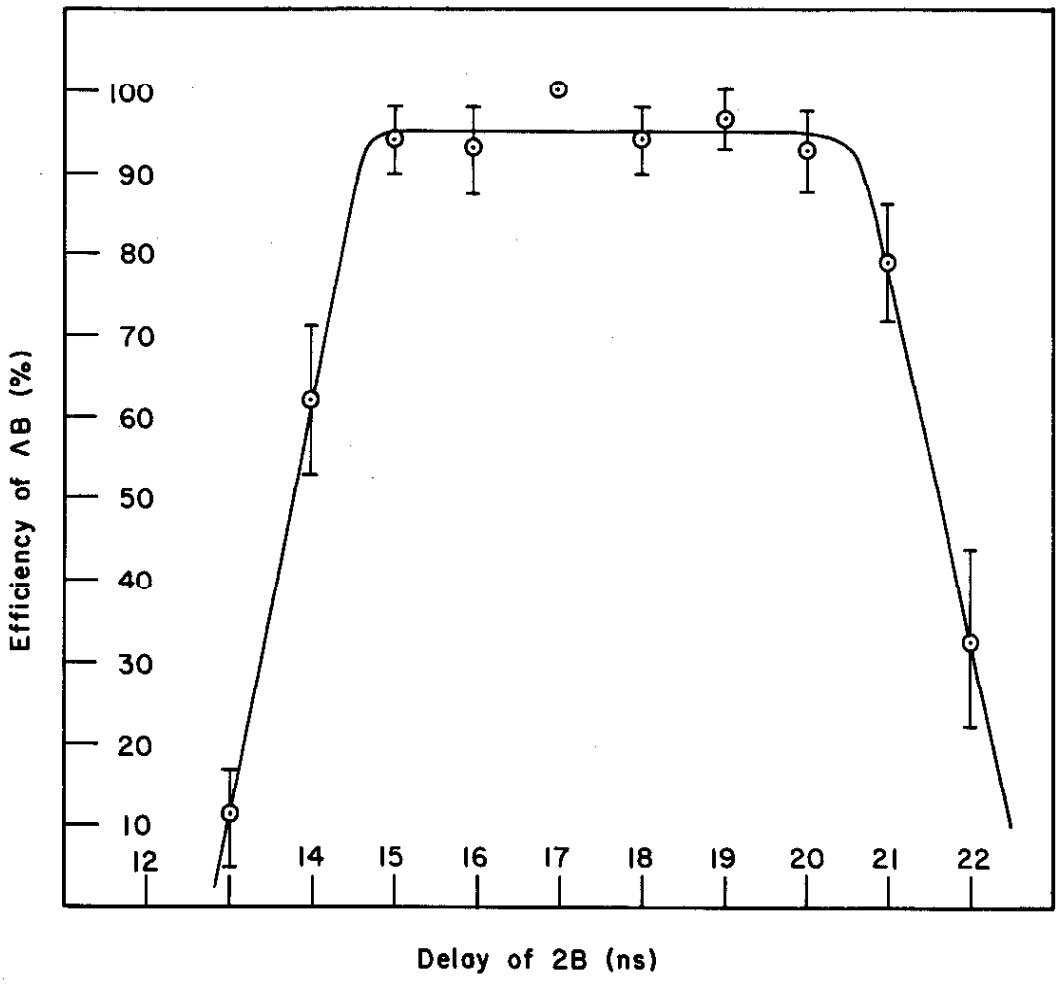

FIGURE 13: Efficiency of the Λ Coincidence

preselection and was found to be of the order of 1%.

The time resolution for the fast gates (TG-1A, TG-1B) is illustrated in figure 14, in which the amplitude of output pulses from protons is plotted versus the delay of a 40 ns wide gating pulse. (The slight asymmetry in the curve resulted from the fact that photo-tube pulses have faster rise times than fall times.)

4.2 Slow Preselection Tests

The amplitude resolutions for the TG-2 discriminators were estimated by observing the sharpness with which a peak produced by protons could be cut. This resolution was about 1 to 2 channels for peaks lying in channel 60.

4.3 Tests of the Pulse-Height Analysis

The linearity of the pulse-height analysis including the fast gates and the Sampling Digitizer, but excluding the photomultiplier tubes, was measured with the mercury pulser. The result, shown in figure 15, illustrates a deviation of ± 1 channel from the best straight line. The zero was deliberately off-set by two channels for all pulse-height inputs, so that the zero drifts could be monitored by the computer. This zero off-set was subtracted in the computer from the actual pulse-height before the data were analyzed.

Spot checks of the stability of the pulse-height analysis with the mercury pulser showed that the system was stable to ± 1 channel for periods up to 5 days and stable to ± 2 channels for periods of several months. The electronics were in an air conditioned room with a temperature usually maintained at 25 ± 5 °C.

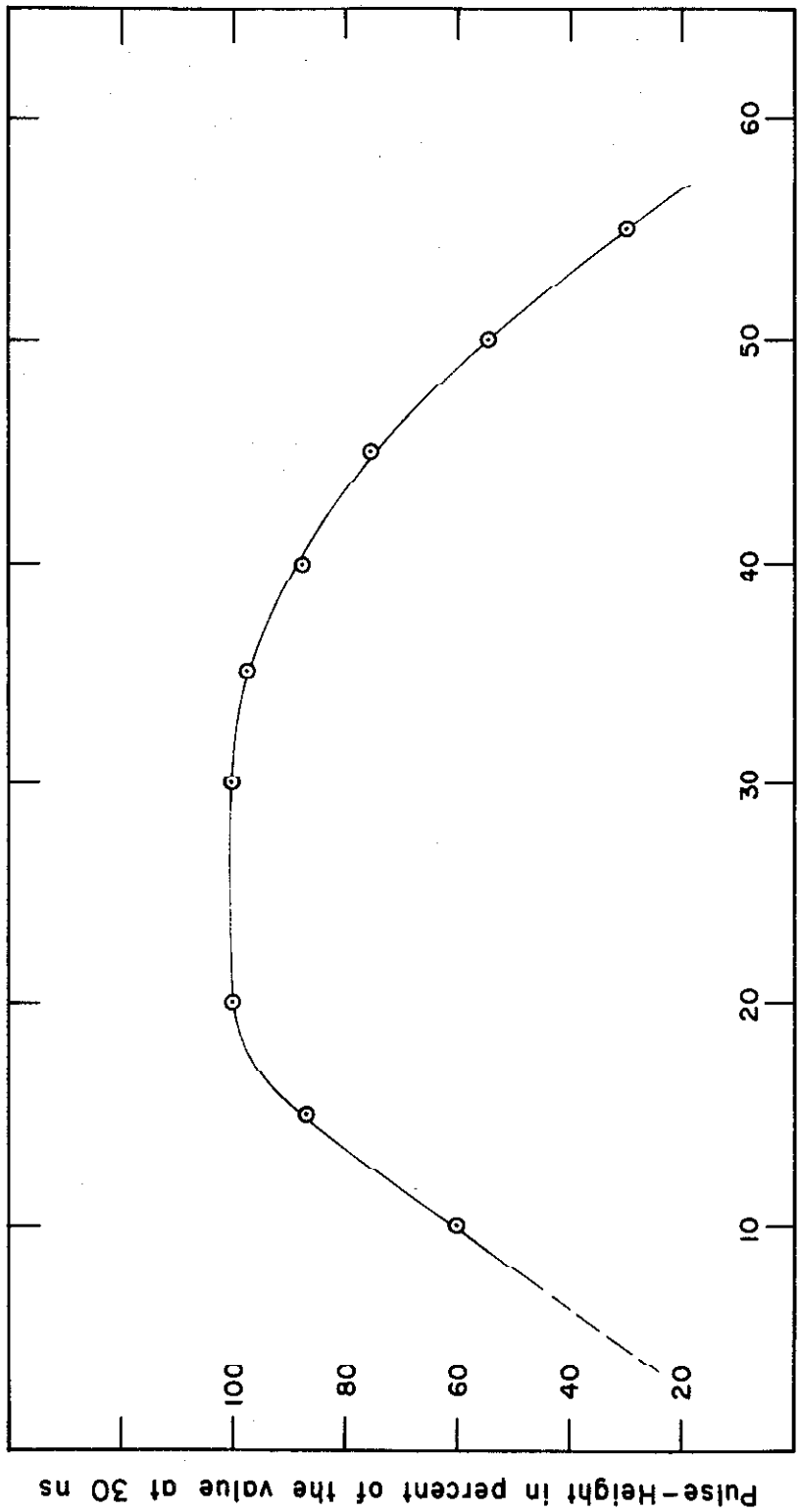

FIGURE 14: Time Resolution of the Fast Gates

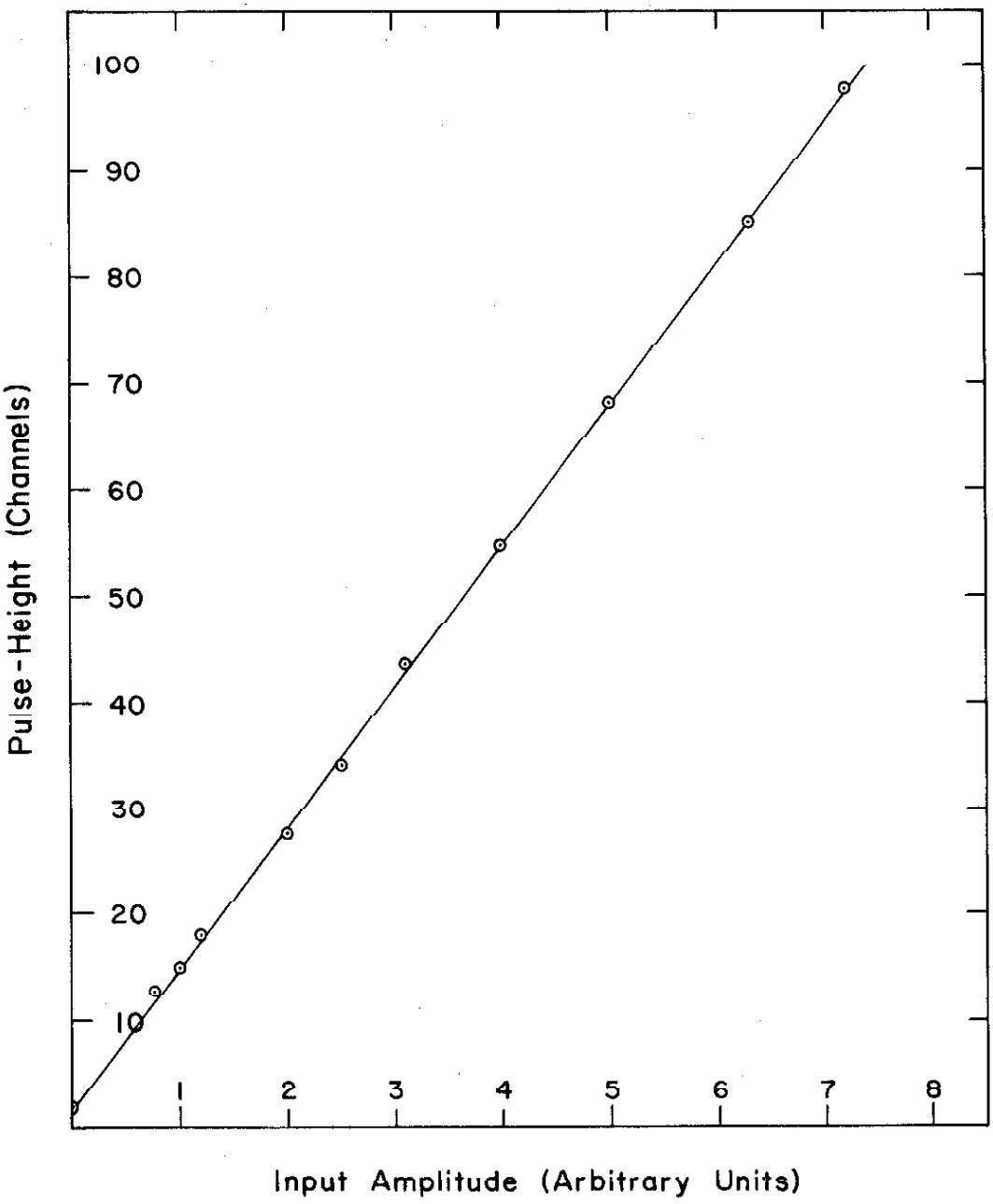

FIGURE 15: Linearity of the Pulse-Height Analysis

4.4 Calibration of the Pulse-Height Analysis

In order to relate the light output (dL/dx) from the scintillators to the output of the Sampling Digitizer, several hundred proton-like events, selected by the slow preselection using the calibration counters (19, 20), were recorded. The computer, using old calibration data and the same statistical techniques used to select kaons, chose those events which fit normally stopping protons. The recorded pulse-heights for these events were then averaged to provide a calibration of the pulse-height analysis. This procedure was iterated if the old calibration was found to be much in error. The side counters (17 and 18) could also be calibrated by placing them in front of the telescope when the proton data were being recorded. The calibration taken above was then extrapolated linearly by about 10% to the dL/dx expected for kaons.

The dL/dx of protons as a function of range was measured by changing the absorber in the telescope, and is shown in figure 16. From 20 g/cm^2 to 68 g/cm^2 the measured and theoretical values agreed within the statistical accuracies of the measurement. The theoretical relationship between dL/dx and dE/dx in the stopping section has also been confirmed.[24]

4.5 Stability and Reliability

Although pulser tests showed that the electronics were stable to within ± 1% over several days, drifts of the calibration sometimes exceeded 5% in a few hours, indicating rapid changes in the photomultiplier tube gains. Because the photomultiplier cathode voltage

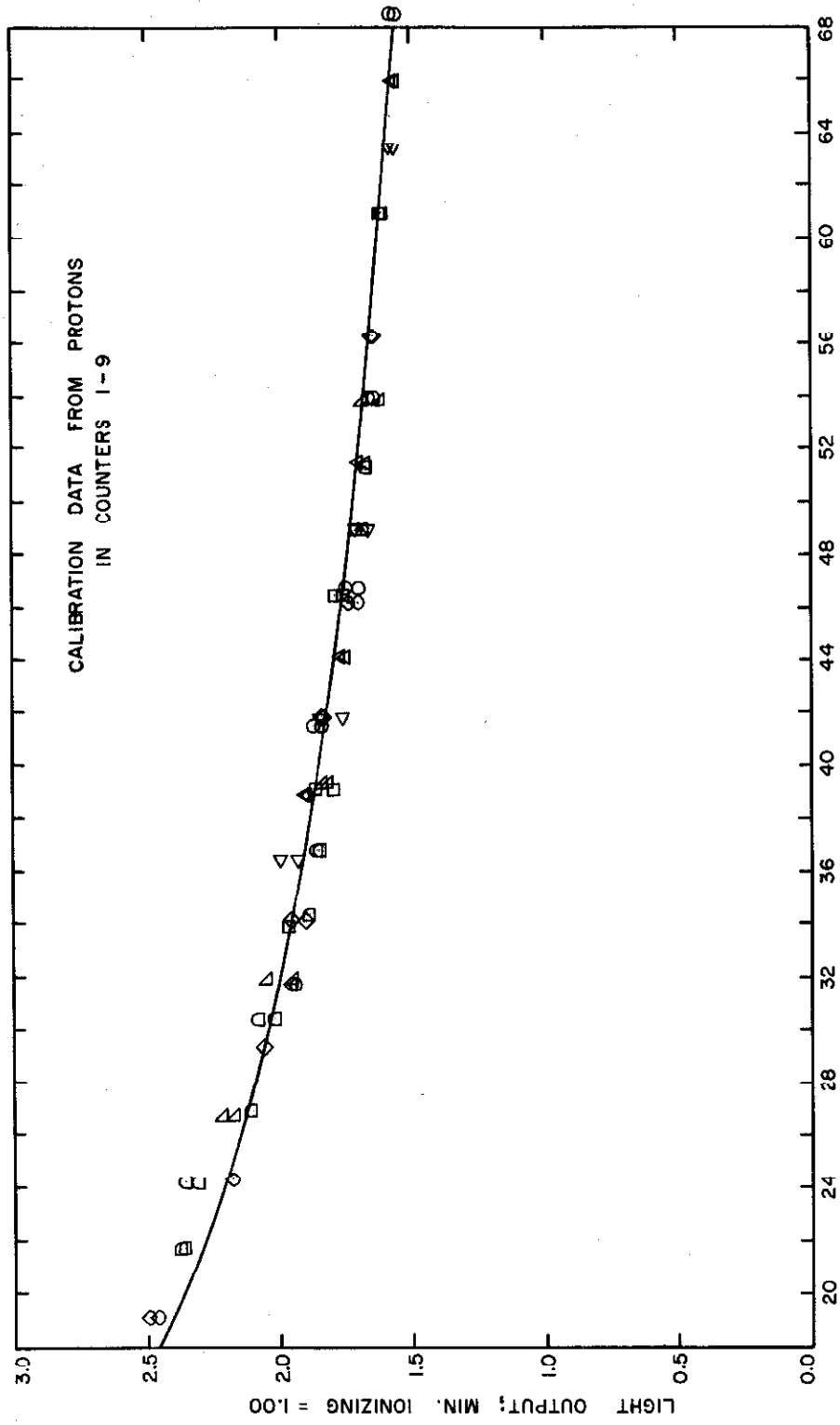

FIGURE 16: A Comparison of Theoretical and Measured Light Outputs vs Particle Range

remained constant to ± 0.04% for several days, changes in this voltage accounted for only ± 0.5% of the gain change. Both temperature variations and counting rate effects on the photomultiplier tubes were suspected. The 5% variations were barely tolerable and definitely compromised the effectiveness of this technique.

Data on the reliability of the electronics has been accumulated since January 1, 1962, and confirmed previous[25] indications of the long life of transistors. Maintenance and repair consumed a negligible amount of time.

Failures among the 3100 transistors in the experiment fell into three categories. First, five transistors failed because of construction faults resulting in short circuits. This type of failure ceased after about nine months during which most of these faults were corrected. Second, marginal circuit design resulted in the failure of several transistors. Two of these failures occurred because one of the transistors in the fast gate (TG-1B) could receive an excessive current pulse when the power was switched off. A current limiting resistor prevented further failures of this sort. The remaining failures occurred in two types of Ransom Research circuits, where sufficient gain margin at high currents was lacking. Third, random failures occurred at a rate of about one transistor for each three months of operation, providing a mean-time-to-failure of over 1,000,000 hours. Such a failure rate was to be expected with germanium transistors, some of which had to operate at high power levels in fast, analog circuit applications.

5.0 CROSS-SECTION DATA

5.1 General

The final data were obtained at the laboratory angles (θ_o), kaon kinetic energies (T_k), and synchrotron end-point energies (E_o) shown in table 4. Runs 1, 4, and 6 supplied the cross-section data for photon energies near 1100, 1200, and 1300 MeV, respectively. The other runs provided data for an excitation curve which checked the validity of the kaon identification.

The kaon yield during a run was given by:

$$Y = N_B \int_{\substack{\text{Telescope}\\ \text{Angles}}} \int_{\text{Target}} \int_{\substack{\text{Photon}\\ \text{Energy}}} R N_\gamma(E_o, k) \rho_p \left(\frac{d\sigma}{d\Omega'}\right) \eta_k \left(\frac{d\Omega'}{d\Omega}\right)_k dk dz d\Omega \quad (10)$$

where:

Y = number of detected kaons during the run.

N_B = number of BIPs (a standard amount of total beam energy) during the run.

R = resolution function of K- and Λ-telescopes.

$N_\gamma(E_o, k)$ = number of photons per unit photon energy per BIP for an end-point energy E_o.

ρ_p = number of protons per cm^3 in liquid hydrogen at its boiling temperature.

$\frac{d\sigma}{d\Omega'}$ = differential cross section in the center of mass for $\gamma + p \rightarrow K^+ + \Lambda$.

η_k = total efficiency for detecting kaons.

$\left(\frac{d\Omega'}{d\Omega}\right)_k$ = solid-angle transformation from the center of mass to the laboratory for kaons.

$d\Omega$ = differential solid-angle of both telescopes in the laboratory.

TABLE 4

Conditions for Kaon Run

Run Number	θ_o (DEG)	T_{ko}(MeV)	E_o MeV
1	37.36	179 ± 18.8	1180
2	37.36	179 ± 18.8	1050
3	37.36	179 ± 18.8	1100
4	40.17	234 ± 16.7	1280
5	40.17	234 ± 16.7	1150
6	41.48	288 ± 15.6	1400
7	41.48	288 ± 15.6	1300
8	41.48	288 ± 15.6	1280
9	41.48	288 ± 15.6	1225

θ_o = Laboratory angle of telescope measured with respect to the photon beam.

T_{ko} = Kinetic energy of a kaon reaching the center of the stopping section. Estimated error = ± 1.3%.

$\pm\Delta T_k$ = Range of kaon kinetic energies defined by stopping section.

E_o = Synchrotron end-point energy.

dz = differential length of target along the photon beam (Z-axis).

dk = differential photon energy.

The integral over the Λ-telescope was performed by Donald Groom,[14] who approximated the K-telescope by a section of a sphere with a solid-angle given by the size of the aperture counter. This calculation resulted in a parameter η_Λ, which gave the probability that the decay proton would be detected by either Λ-telescope, considering only the geometry and the kinematics of the kaon production and the Λ decay. Values of η_Λ are given in table 7.

The yield integral could then be approximately separated as follows:

$$Y \cong \left\{ N_B \int_{\substack{\text{K-Telescope}\\ \text{Angles}}} \int_{\text{Target}} \int_{\substack{\text{Photon}\\ \text{Energy}}} R_k N_\gamma(E_o, k) \left(\frac{d\Omega'}{d\Omega}\right)_k dk dz d\Omega_k \right\} \times \eta_\Lambda \bar{\eta}_k \rho_p \left(\frac{\overline{d\sigma}}{d\Omega'}\right) \tag{11}$$

where the average of the differential cross-section $\frac{\overline{d\sigma}}{d\Omega'}$ and the average efficiency $(\bar{\eta}_k)$ have been factored out.

5.2 Integral Over Photon Energy and K-Telescope

The photons produced by bremsstrahlung in the synchrotron had an energy spectrum given by:

$$N_\gamma(E_o, k) = \frac{W B(k, E_o)}{E_o\, k} \tag{12}$$

where values of $B(k, E_o)$ can be found in reference 44. Because $B(k, E_o)$ is normalized so that

$$\int_0^{E_o} B(k, E_o)dk = E_o \tag{13}$$

the constant W becomes the total energy in the photon beam per BIP. The number of BIPs during a run and the value of W were determined as follows:

The photon beam was absorbed by an ion chamber, which produced a charge output proportional to the energy in the photon beam. This charge was accumulated by the Beam Integrator, which provided a pulse called the BIP whenever the total charge exceeded a pre-set level. To within a small rounding error, the total energy during a run was proportional to the number of BIPs. A Wilson Quantameter[26] provided an absolute calibration between the energy in the beam and charge. The Beam Integrator was calibrated using a stable charge generator.

The details of the integrals over the K-telescope angles, the target, and photon energy are discussed in Appendix C. These integrals provided the angular and energy resolution functions shown in figures 17 and 18. After evaluating these integrals, the yield can be written as:

$$Y = \frac{N_B \eta_T \overline{\frac{d\upsilon}{d\Omega'}}}{K} \tag{14}$$

where $K = \dfrac{E_o}{\rho_p W I}$

$$I = \int_{\substack{\text{K-Telescope}\\ \text{Angles}}} \int_{\text{Target}} \int_{\substack{\text{Photon}\\ \text{Energy}}} R_k \frac{B(k, E_o)}{k} \left(\frac{d\Omega'}{d\Omega}\right) dk dz d\Omega_k$$

$$\eta_T = \eta_\Lambda \overline{\eta}_k$$

Values for K and for the parameters used in calculating K are given in table 5, with the functional dependence on E_o being shown by the smooth curves in figure 19.

5.3 Efficiencies

The efficiencies were divided into three categories: those efficiencies independent of the run, those depending only on the K-telescope configuration, and those depending on the specific run. In the latter category the only correction was that caused by accidentals.

5.3.1 Efficiencies Independent of the Run

These efficiencies are summarized in table 6. Because the Λ-particle could decay in to π^o + n, which was not detected, the branching ratio (η_B) for the π^- + p decay mode had to be included as an efficiency. Also, the data had to be corrected for the detection of the π^-. The geometrical efficiency for detecting both the proton and the π^- in different Λ-telescopes was estimated to be 4.2% for the 1200 MeV point; the probability of detecting only the π^- was about 1%. The number of times that both Λ-telescopes were triggered in coincidence with a kaon-like particle in the K-telescope was found to be $2 \pm 0.5\%$. Because this rate was over an order of magnitude above the probability for accidental events of this type, the ratio of 2 to 4.2 was interpreted as the probability that the Λ-telescope Cerenkov counters did not detect the π^-. Because the events showing coincident particles in both Λ-telescopes were discarded, the data had to be corrected by a factor:

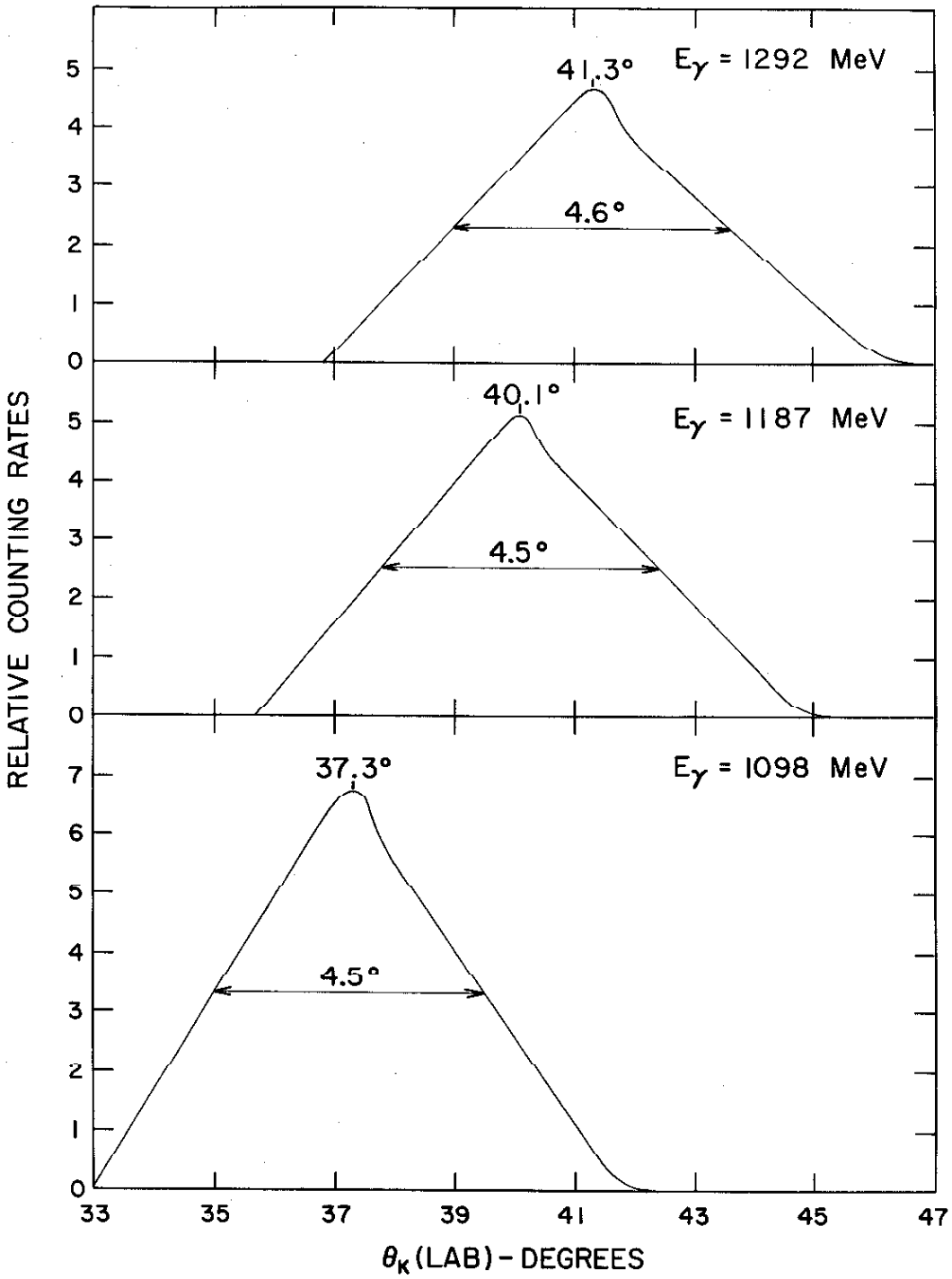

FIGURE 17: Angular Resolution of the K-Telescope

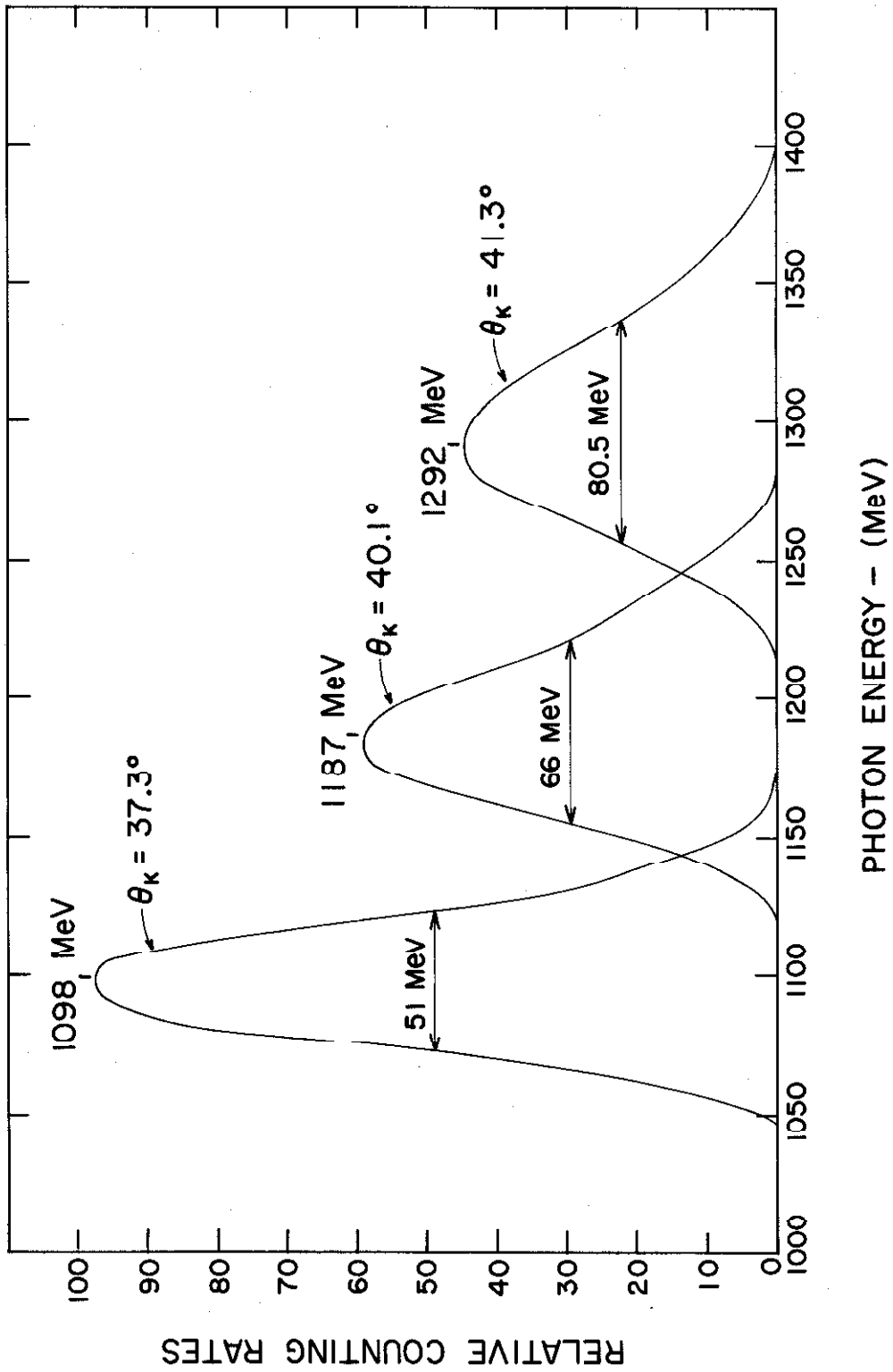

FIGURE 18: Photon Energy Resolution of the K-Telescope

TABLE 5

Parameters for the Calculation of K

Run Number	E_o(MeV)	ρ_p (cm^{-3})(41)	W(MeV/BIP)	I(cm-sr)
1	1180	4.25×10^{22}	$(1.218 \pm 1\%) \times 10^{13}$	$(1.34 \pm 1\%) \times 10^{-2}$
2	1050	4.25×10^{22}	$(1.209 \pm 1\%) \times 10^{13}$	$< 10^{-5}$
3	1100	4.25×10^{22}	$(1.211 \pm 1\%) \times 10^{13}$	$(0.442 \pm 1\%) \times 10^{-2}$
4	1280	4.25×10^{22}	$(1.222 \pm 1\%) \times 10^{13}$	$(1.025 \pm 1\%) \times 10^{-2}$
5	1150	4.25×10^{22}	$(1.213 \pm 1\%) \times 10^{13}$	$< 10^{-5}$
6	1400	4.25×10^{22}	$(1.227 \pm 1\%) \times 10^{13}$	$(0.951 \pm 1\%) \times 10^{-2}$
7	1300	4.25×10^{22}	$(1.223 \pm 1\%) \times 10^{13}$	$(0.356 \pm 1\%) \times 10^{-2}$
8	1280	4.25×10^{22}	$(1.222 \pm 1\%) \times 10^{13}$	$(0.159 \pm 1\%) \times 10^{-2}$
9	1225	4.25×10^{22}	$(1.220 \pm 1\%) \times 10^{13}$	2.92×10^{-6}

TABLE 6

Efficiencies Independent of the Run

Type	Value
Branching of Λ decay (η_B)	0.677 ± 0.01
Effect of π^- in Λ-Telescope (η_{π^-})	0.985 ± 0.01
Decay particle veto (η_{DV})	0.716 ± 0.016
Counter spike (η_s)	0.97 ± 0.01
Target losses (η_{TL})	0.968 ± 0.016
TC-2 bias losses (η_{TC-2})	0.97 ± 0.03
U > 2.0 bias loss (η_u)	0.974 ± 0.023

$$\eta_1 = \eta_B \eta_{\pi^-} \eta_{DV} \eta_s \eta_{TL} \eta_{TC-2} \eta_u = 0.422\ (1 \pm 5.08\%)$$

(Total errors are the square-root of the sum of the squares of the individual errors.)

$$\eta_{\pi^-} = 1 - \frac{2}{4.2}\left(\frac{4.2 - 1}{100}\right) = 0.985 \qquad (15)$$

Because this correction was small, it was assumed to be the same for all runs.

If a charged particle from a kaon decay passed through the end counter, the event would be rejected by the slow preselection. Also, because no provision was made in the calculation of U and S for a decay particle in any other counters except those in the stopping section, a backward-travelling decay particle which entered counters 11 or 12 would cause the event to be rejected. The probability of such events was calculated by a Monte Carlo program[27] and resulted in the efficiency η_{DV}.

Small kaon losses also resulted from the increased light output near the counter light-pipes (η_s), [13] boiling in the hydrogen target (η_{TL}),[43] the amplitude windows on the first eight counters (η_{TC-2}), and the bias that U be less than 2.0 (η_u).

5.3.2 Efficiencies Dependent Only on Telescope Configuration

The values of these efficiencies for the three telescope configurations are given in table 7.

Kaons could interact with the hydrogen and carbon nuclei of the K-telescope counters and absorber, resulting in large pulses and large angle scattering which would cause the particle to be lost. The cross-section for scattering from hydrogen through an angle greater than 12° has been found to be 16 ± 3.2 mb for kaon energies from 40 MeV to 275 MeV.[28,29] The total cross-section for scattering from carbon with an angle greater than 22.1° for a kaon

TABLE 7

Efficiencies Dependent Only on Telescope Configuration

Run Number	1 - 3	4 - 5	6 - 9
Λ-Telescope Geometry (η_Λ)	0.366±0.0037	0.451±0.0045	0.512±0.0051
Absorption (η_A)	0.836±0.032	0.766±0.046	0.694±0.060
Decay in flight (η_{DF})	0.629±0.037	0.655±0.034	0.690±0.034
Counter 12 Saturation (η_{12})	0.928±0.017	0.928±0.017	0.974±0.017
Multiple Scattering (η_{ms})	0.97 ±0.01	0.97 ±0.01	0.97 ±0.01
Truncation of S (η_S)	0.9997	0.9970	0.9937
$\eta_2 = \eta\ \eta_A \eta_{DF} \eta_{12} \eta_{ms} \eta_S$	0.173 × (1 ± 7.40%)	0.203 × (1 ± 8.27%)	0.230 × (1 ± 10.2%)

(Total errors are the square-root of the sum of the squares of the individual errors.)

TABLE 8

Accidental Correction

Run Number	Accidental Correction (η_{ACC})
1	0.832 ± 0.015
2	0.846 ± 0.015
3	0.832 ± 0.015
4	0.831 ± 0.016
5	0.840 ± 0.015
6	0.856 ± 0.022
7	0.849 ± 0.022
8	0.901 ± 0.017
9	0.855 ± 0.022

energy of 190 MeV was found to be 96.5 ± 8.5 mb.[30] Because the hydrogen cross-section was not strongly energy dependent and because for most of their path length the kaons had energies near 190 MeV, the carbon cross-section was assumed to be a constant 96.5 mb for all kaon energies in the K-telescope. From these cross-sections and from the known chemical composition of the K-telescope, the absorption correction (η_A) in table 7 was calculated.

The decay of kaons in-flight between the target and the stopping section provided another loss mechanism. Including relativistic time dilation, this decay correction is given by:

$$\eta_{DF} = \exp\left[-\frac{m}{\tau c}\int_0^R \frac{dx}{p}\right] \qquad (16)$$

where η_{DF} = probability of in-flight decay

m = kaon mass

τ = kaon lifetime

c = speed of light

R = distance from the target to the middle of the stopping section

p = kaon momentum

The decay corrections shown in table 7 were calculated from equation 16 using a kaon lifetime of 12.29 ± 0.08 ns and a kaon mass of 493.8 MeV.[42]

A correction also had to be made for the loss of δR caused by saturation effects in counter 12 (η_{12}). Because all events saturating the pulse-height analyzer were rejected, particles which stopped in the first 3 to 7% of the stopping section were lost.[27]

The loss of particles from the K-telescope because of multiple scattering (η_{ms}) was estimated to be 3%.[14] A small correction (η_S) was made for the truncation of S.

5.3.3 Accidental Correction

The methods of section 3.5 using the constants of table 3 were applied to the accidental monitor counting rates. The results are shown in table 8.

During a typical run, the accidental correction resulting from the Λ-telescope Cerenkov counters was 4.6%, from the gate accidentals and K-coincidence circuit dead time 1.8%, from the Sampling Digitizer dead time 6.3%, and from the dead time of the Λ-coincidence circuits 3.2%. Other accidental effects were less than 0.2%.

5.4 Results

In order to check on the elimination of background and on the theoretical resolution functions, several runs were made at reduced synchrotron end-point energies. The results of these excitation curve runs are summarized in table 9, with theoretical and experimental values being compared in figure 19. The best fit for theoretical and experimental data occurred if the end-point energy was assumed to be 5 MeV higher than that indicated by the synchrotron Beam Energy Meter. This displacement is not inconsistent with a 15 MeV shift suspected by Peck.[20] Uncertainties in the kaon range and in the dependence of energy on range led to a ± 2.5% error in the kaon energy, which was reflected as an error in photon energy of ± 5.3 MeV at E_γ = 1098 MeV, ± 8.7 MeV at E_γ = 1187 MeV, and

TABLE 9

Excitation Curve Data

Run Number	E_o(MeV)	E_γ(MeV)	$N_{25} \pm \sqrt{N_{25}}$	$b \pm \Delta b$	$Y \pm \Delta Y$	N_B	η_T	$\frac{Y}{N_3 \eta_T}$	Relative Rate	Relative Value of 1/k
1	1185	1098 ±25.5	1385 ±37.2	0.378 ±0.036	861 ±54.4	17,495	6.07%	0.814 ±6.31%	1.005 ±0.063	1.005
2	1055		153 ±12.4	1.00 ±0.01	0 ±0.01	5,775	6.18%	0	0	0.002
3	1105		65 ±8.05	0.66 ±0.09	22.1 ±6.1	968	6.07%	0.376 ±27.6%	0.463 ±0.128	0.40
4	1285	1187 ±33.0	1540 ±39.2	0.165 ±0.038	1290 ±67.5	30,131	7.15%	0.595 ±5.23%	1.005 ±0.052	1.005
5	1155		20 ±4.46	0.95 $^{+0.05}_{-0.14}$	1 ±1	3,707	7.22%	0.004 ±100%	0.006 ±0.006	0.001
6	1405	1291 ±40.3	1522 ±39.0	0.063 ±0.053	1430 ±89.4	33,752	8.35%	0.509 ±6.22%	1.005 ±0.062	1.005
7	1305		79 ±8.9	0 $^{+0.05}_{-0.0}$	77.5 ±9.1	4,532	8.26%	0.211 ±11.7%	0.416 ±0.049	0.46
8	1285		35 ±5.91	0.11 $^{+0.16}_{-0.11}$	31.2 ±7.1	2,893	8.79%	0.123 ±22.8%	0.243 ±0.055	0.245
9	1230		2 ±1.41	0 $^{+0.3}_{-0.0}$	2 ±1.5	4,012	8.34%	0.006 ±75%	0.012 ±0.009	0.005

TABLE 10

Cross-Section Data

Run Number	E_o(MeV)	E_γ(MeV)	θ_k(lab-deg)	ϵ_k(c.m.-deg)	$Y = \Delta Y$	N_B	K(μb/sr)	$\eta_T \pm \frac{\Delta \eta_T}{\eta_T}$	$\frac{d\sigma}{d\Omega}$ (μb/sr)	Statistical Error	RMS Systematic Error
1	1185	1098 ±25.5	37.3 ±2.25	89.9 ±5.1	861 ±54.4	17,495	0.1705 ±2%	0.0607 ±9.15%	0.139	±6.31%	± 9.4%
4	1285	1187 ±33.0	40.1 ±2.25	90.2 ±4.5	1290 ±67.5	30,131	0.240 ±2%	0.0715 ±9.89%	0.143	±5.23%	±10.2%
6	1405	1292 ±40.3	41.3 ±2.30	89.8 ±4.3	1430 ±89.4	33,752	0.282 ±2%	0.0835 ±11.7%	0.143	±6.22%	±12.1%

E_o = synchrotron end-point energy

E_γ = central value of photon energy

$\pm\Delta E_\gamma$ = ± half-width at half-maximum of photon energy resolution function

θ_k(lab) = central value of kaon laboratory angle with respect to photon beam

$\pm\Delta\theta_k$(lab) = ± half-width at half-maximum of laboratory angular resolution function

θ_k(c.m.) = central value of kaon center of mass angle

$\pm\Delta\theta_k$(c.m.) = half-width at half-maximum of center of mass angular resolution function

N_{25} = number of events with $U \leq 2.0$ and $S \leq 25$

b = fraction of N_{25} which are not kaons

$\pm\Delta b$ = statistical error in b

$\frac{d\sigma}{d\Omega} = YK/N_B\eta_T$

$\eta_T = \eta_1\eta_2\eta_{ACC}$

$Y = (1-b)N_{25}$

$\Delta Y = N_{25}\sqrt{(\Delta b)^2 + \frac{(1-b)^2}{N_{25}}}$

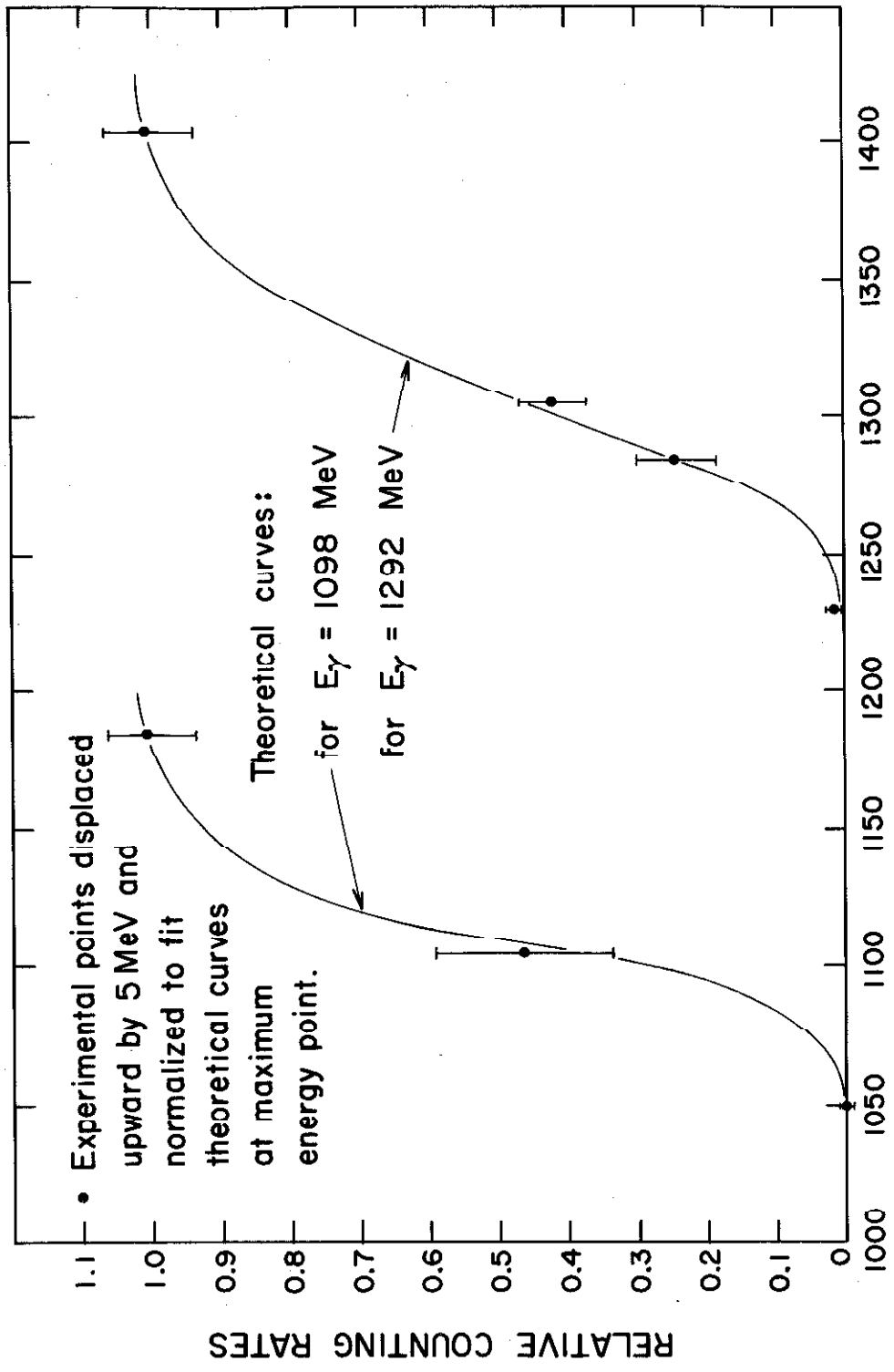

FIGURE 19: Thecretical and Experimental Excitation Functions

$\pm$ 11.6 MeV at E_γ = 1291 MeV.

Because the predicted and measured excitation functions agreed within statistical errors, the telescope resolution functions appear confirmed. The lack of counts below the kaon kinematic threshold indicated that the remaining background was less than 1%. Furthermore, the average fraction of the kaon events showing a side counter pulse produced by a decay particle was 0.294 $\pm$ 0.02, in agreement with the theoretical value of 0.283 $\pm$ 0.023 obtained from simulated kaons generated by a Monte Carlo program.[27]

The differential cross-section data are shown in table 10. The cross-section remained nearly constant at a value of 0.14 μb/sr for photon energies between 1098 MeV and 1291 MeV. These values are shown in table 11 and figure 20, which compare the results of this experiment with previous cross-section measurements. Because the lower energy values agreed well with the work of Anderson, et al.,[8] Sadoff, et al.,[11] Thom, et al.,[9] and Peck,[10] considerable confidence can be placed in the absolute calibration.

Table 10 also shows the RMS errors involved. The statistical errors resulted from the counting statistics on the number of events and from uncertainties in the background correction (see section 2.4). The systematic errors, provided by uncertainties in the efficiencies and in the resolution functions, ranged from $\pm$ 9.4% for a photon energy of 1098 MeV to $\pm$ 12.1% at 1292 MeV. The systematic errors claimed for previous work were about $\pm$ 10%.

TABLE 11

Differential Cross-Section

Data Near θ_k (c.m.) = 90°

Source	E_γ(MeV)	θ_k(c.m.-deg.)	$\frac{d\sigma}{d\Omega}$ in 10^{-31} cm^2/sr
Anderson, et al.[8]	934	90.0	0.55 ± 0.04
	1004	88.6	1.54 ± 0.09
	1024	94.2	1.45 ± 0.11
	1054	89.7	1.57 ± 0.09
	1080	90.0	1.58 ± 0.08
	1130	90.0	1.42 ± 0.13
Donoho and Walker[2]	960	90	1.18 ± 0.35
	1000	90	1.46 ± 0.23
	1060	90	1.47 ± 0.26
Sadoff, et al.[11]	1160	90	1.44 ± 0.10
Thom, et al.[9]	1200	90	1.53 ± 0.09
Peck[10] (Extrapolated from 85°)	1200	90	1.35 ± 0.18
This experiment	1098	89.8	1.39 ± 0.088
	1187	90.2	1.43 ± 0.075
	1292	89.8	1.43 ± 0.089

(Errors are statistical only.)

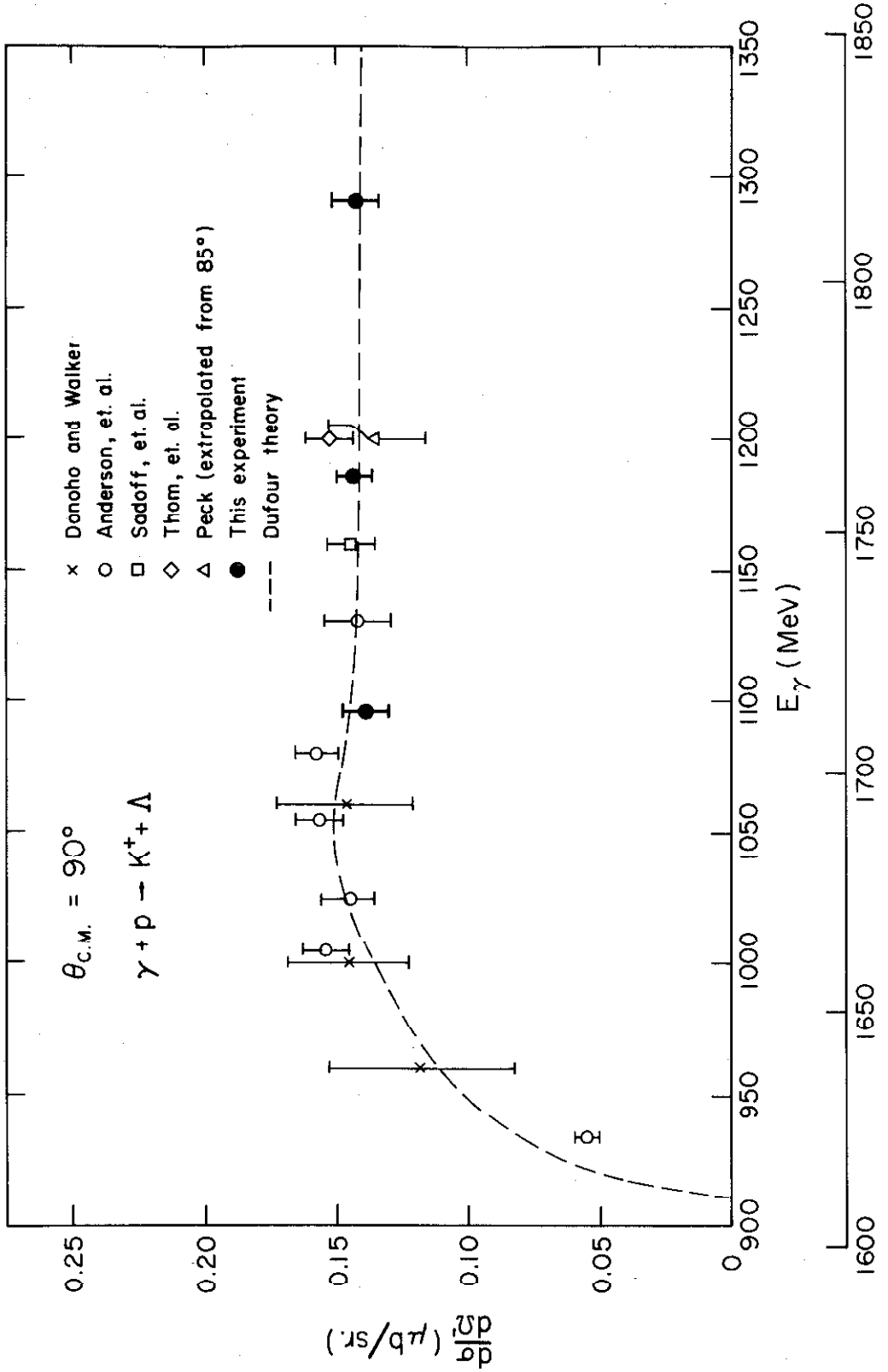

FIGURE 20: Differential Cross-Section at 90° in the Center of Mass for $\gamma + P \rightarrow K^+ + \Lambda$

6.0 CONCLUSIONS

6.1 Theoretical Considerations

Several phenomenological theories have been devised to explain $K\Lambda$ photoproduction.[31-36] Peck[10] found that the model of Kuo[35] and Beauchamp and Holliday[36] did not fit the measured angular distribution at E_γ = 1200 MeV and predicted the wrong sign for the Λ polarization. Furthermore, both Groom and Peck independently were unable to reproduce the numerical results of the Hatsukade and Schnitzer theory,[31,32] preventing it from being continued to energies above the published[32] 1060 MeV case. Thus, I chose the model of Dufour and Gourdin[33,34] for the comparison of the results of this experiment with theoretical predictions.

In this model, the production amplitudes were calculated using the Born approximation for suspected dominant single-particle exchanges, with the $K^*_{1/2}$ (1$\bar{}$855) and $N^*_{1/2}$ ($5/2^+$, 1688) resonant states being added explicitly using Breit-Wigner forms. A non-zero width was kept for the latter resonance, but not for the former which does not occur in the physical region.

The theory had seven parameters to be fit to the experimental data. Dufour recently[37] included in the fit the angular distribution data of Peck[10] at 1200 MeV with previously existing[34] cross-section and polarization data. Sixteen equally valid choices for the parameters of the fit resulted if the Λ anomalous magnetic moment (μ_Λ) and the width of the $N^*_{1/2}$ ($5/2^+$, 1688) were treated as relatively free parameters. To restrict this large choice, μ_Λ was chosen equal to -0.955 nuclear magnetons in agreement with the eightfold way[38]

and as a value intermediate between two conflicting experimental results.[39,40] Choosing a width for the $N^*_{1/2}(5/2^+, 1688)$ resonance equal to 100 MeV reduced the number of available parameter sets to one. The theory using these parameters was continued to energies above 1200 MeV by Donald Groom using the IBM 7094 computer. The dotted curve shown in figure 20 was obtained in this manner.

From figure 20, it is apparent that the Dufour theory gives good agreement with the differential cross-section measured at a center of mass angle of 90°. The theory predicts a slight rise in the cross-section near a center of mass energy corresponding to the mass of the $N^*_{1/2}(5/2^+, 1688)$. The experimental data are certainly consistent with the rise, although the errors are somewhat large to state definitely that such a rise really exists. In the region of this experiment, the theory predicts only small changes in the differential cross-section; this fact is now experimentally confirmed. The theory also predicts the correct sign of the Λ-polarization, although the magnitude is consistently below the experimental data.[14]

In order to provide a non-zero Λ-polarization, the $N^*_{1/2}(5/2^+, 1688)$ must contribute to the production amplitudes in the Dufour theory.[34] However, the fit to the angular distribution data[10] at forward angles at 1200 MeV is significantly better if the $N^*_{1/2}(5/2^+, 1688)$ state is excluded.[14,37]

From the cross-section data alone, the presence of effects from the $N^*_{1/2}(5/2^+, 1688)$ resonance remain unconfirmed. The Dufour theory, including the resonance to explain the polarization rise near E_γ = 1100 MeV, predicts differential cross-section values which

agree well with this experiment at 90° but less well at more forward angles. The safest conclusion to be drawn from this experiment is that the differential cross-section at 90° in the center of mass remains nearly constant for photon energies from 1100 MeV to 1300 MeV. Also, the absolute magnitude of the differential cross-section measured at Cornell by a different technique for energies between 1100 MeV and 1200 MeV has been verified within 10% systematic errors.

6.2 General Comments

Now that this experiment has been completed and shown to detect kaons predictably, a few remarks on the general approach are in order.

The high efficiency for detecting kaons with associated Λ decay was achieved, although by the time that the experiment was completed the order of magnitude increase in the synchrotron photon beam intensity reduced the importance of this reason. However, the relatively high counting rate for Λ events did make it feasible to measure the Λ polarization with a statistical accuracy of about ± 0.07 at several different photon energies.

This experiment also provided valuable experience in designing and operating a complex experiment in a small laboratory. Because limited personnel were available for repair and maintenance, the equipment had to be designed with sufficient reliability so that virtually no maintenance would be necessary. At least in this experiment, the reliability of the equipment was not a limiting factor,

indicating that increased complexity should not be feared if high standards are maintained in the design of engineering details.

Although this experiment finally produced data reliably and rapidly, five years were required to build the equipment, write the computer programs, and wait for reliable synchrotron and computer operation. Anyone planning similar experiments in the future should not underestimate the time required to design and build dozens of electronic circuits and to write thousands of words of computer programs. Therefore, we must seriously question whether a system of this complexity is a reasonable project for two graduate students to undertake virtually without assistance in the engineering and computer problems. Complex systems using computers directly are only efficient when sufficient back-up personnel are available so that the flexibility, speed, and powerful data handling capability inherent in such systems can be rapidly applied. If the resources of a laboratory are too limited, then the time required to implement such a powerful technique may exceed the time justified by the experiment.

APPENDIX A

Some Considerations in the Design of the Experimental Method

Given the requirement that a counter telescope be used for the kaon identification, the following considerations determined the choice of the number of counters used in the slow preselection and the general direction for the data analysis.

In this experiment plastic scintillation counters were used to measure the rate of energy loss of charged particles. The amount of light produced per unit length (dL/dx) of such a counter is related to the rate of energy loss (dE/dx) by:[24]

$$dL/dx = Ka \ln\left[1 + \frac{1}{a} dE/dx\right] \qquad (17)$$

where K is a proportionality constant independent of dE/dx and a is an empirical constant approximately equal to 40 MeV/cm.

Unfortunately the light output was not a unique value, but was subject to statistical fluctuations.[45] The width of the pulse-height distribution at the photomultiplier anode was further increased by statistical variations in the number of electrons leaving the photocathode. Also any variations in the gain of the photomultiplier resulting from high voltage shifts, counting rate changes, or temperature fluctuations would cause further widening of the pulse-height distribution. A typical peak produced by 300 MeV protons in one of our 2 cm thick counters could be approximately fitted by a Gaussian distribution with a root-mean-square width of 10%.

Because theoretical analysis[14,45] did not predict much difference in the shape of the distributions for pions, protons, and kaons in our telescope, all pulse-height distributions were approximated* by Gaussians with widths of 10%.

These statistical fluctuations, which were the principal concern in the design of the bias windows of the slow preselection, resulted in two conflicting requirements. First, the bias windows, centered about the dL/dx expected for kaons, had to be sufficiently wide so that the kaon counting rate would not be drastically reduced and the efficiency would not be critically dependent on electronic gains and biases. On the other hand, the efficiency for accepting protons and pions had to be low enough to prevent the computer from being flooded with non-kaon events.

Because the light outputs for pions and protons differed from the light output for kaons by the same order as the statistical fluctuations, several measurements of the dL/dx of a particle had to be made in order to reduce the statistical undertainties to a level consistent with the above requirements, resulting in bias windows set in several counters. The choice of the number of counters was principally determined by the desired proton rejection ratio for a fixed kaon efficiency. In figure 21 the probability (η_p) for accepting a proton as a function of the number of counters (N) is shown for the case where the probability of accepting a kaon (η_k) was fixed at 0.95. For this calculation the pulse-height distributions in different

---

* This approximation holds when the particles are sufficiently ionizing so that the Landau tails are negligible.

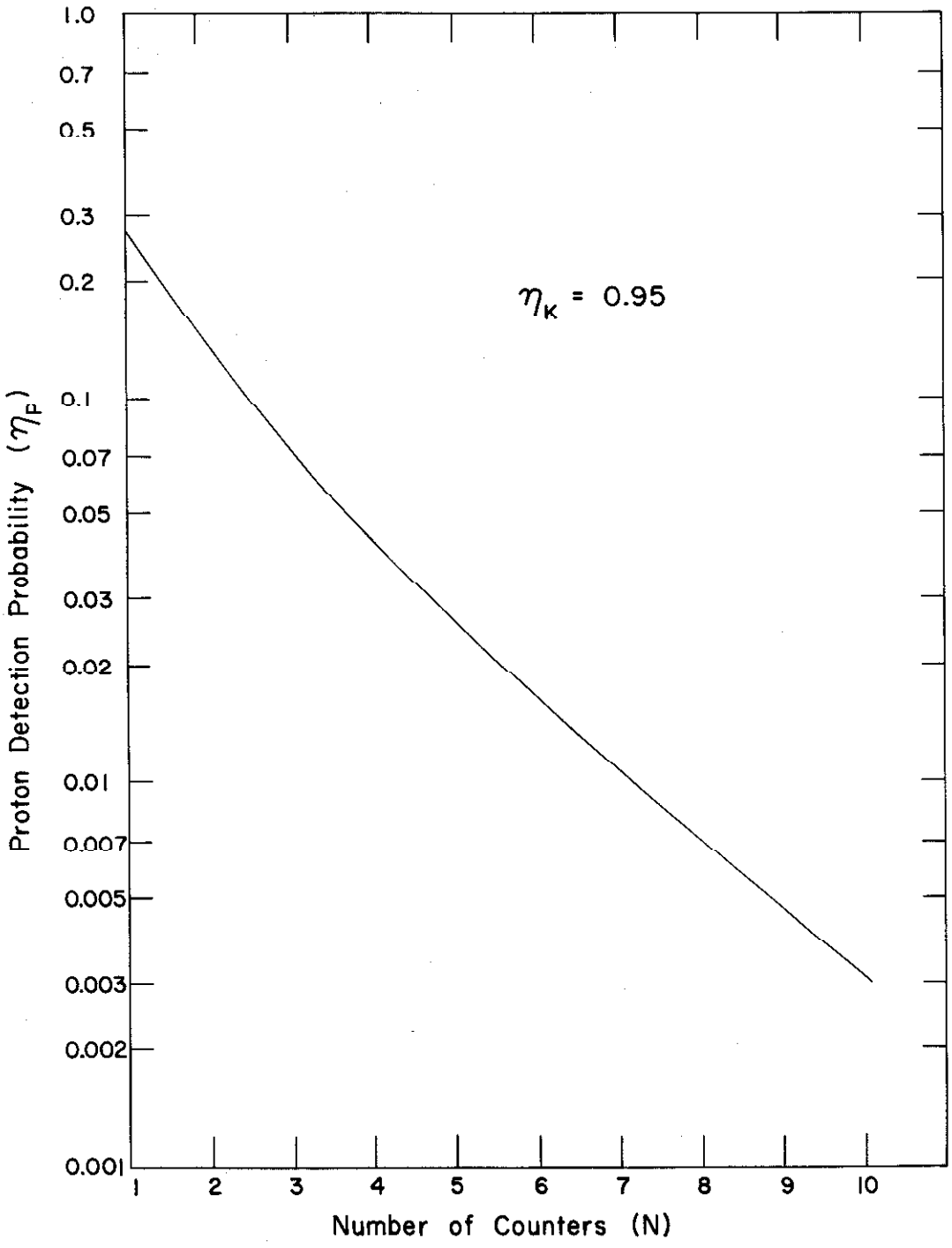

FIGURE 21: Dependence of the Proton Detection Probability on the Number of Counters Used for Amplitude Windows

counters were assumed to be statistically independent, and the kaon and proton light outputs in all counters were approximated as being the values for a range of 35 g/cm^2. Taking account of the fact that there are both upper and lower biases with a stability of about 5%, the expected stability of η_k was 1% to 2%. Because such stability requirements limited the value of η_k to 95% or higher, figure 21 provided a reasonable estimate of the amount of proton rejection possible by the bias method for particles of fixed range, neglecting the skewness of the pulse-height distributions. The skewness decreased η_k, making the particle separation problem more difficult.

From figure 21 it would appear that with a sufficient number of counters the bias method alone could separate kaons from protons. Unfortunately, the kaon range changed by 12 g/cm^2 for incident energies between 215 MeV and 255 MeV, resulting in a variation in the most probable value of the light output. For counters more than about 20 g/cm^2 from the front of the telescope, this spread in light output rapidly became comparable to and then greater than the statistical fluctuations. For these counters, the curve in figure 21 would no longer be applicable, and the bias method became considerably less efficient in rejecting protons.

Part of the solution to the above problem could be to mix with the output of each counter a small fraction of the light output from the stopping section. Because the feedback pulse-height resulting from a particle with a long range would be increased compared to a particle with a short range, the effect of the range variation would tend to be cancelled. This solution was not as attractive as

first appeared, because the light from charged kaon decay particles could add to the signal from the stopping section and once again smear the distributions.

As a result, the bias method operated efficiently only for counters in which the particles had a range in excess of about 20 g/cm^2. Because the counters had to be nearly 2 cm thick in order to have good resolution, and because the range of a 235 MeV kaon was 48 g/cm^2, at most 13 counters made of scintillator plastic with a density of 1.054 g/cm^3 could be used. Even if there were no other difficulties with the bias method, thirteen would be only a barely sufficient number of counters to reduce the background from the 100 to 200 times more numerous protons to 5% of the kaon rate.

Furthermore, the bias method did not reject some fast protons which interacted after leaving the counters in which biases were applied. In figure 22 the dL/dx versus range of a kaon is compared to the dL/dx of protons with 20. 30. and 40 g/cm^2 more range than the kaon. These examples all lie within one standard deviation of being a kaon over most of the range for which the bias method was efficient. If one of these protons were to interact later in the telescope so that it did not pass through the veto counter, then it would probably be accepted as a kaon. Experience has shown that events of this type can be an order of magnitude more numerous than kaons.

Clearly the bias method suffered from the restriction that it could only be applied to counters near the front of the telescope where range variations did not cause large changes in the dL/dx.

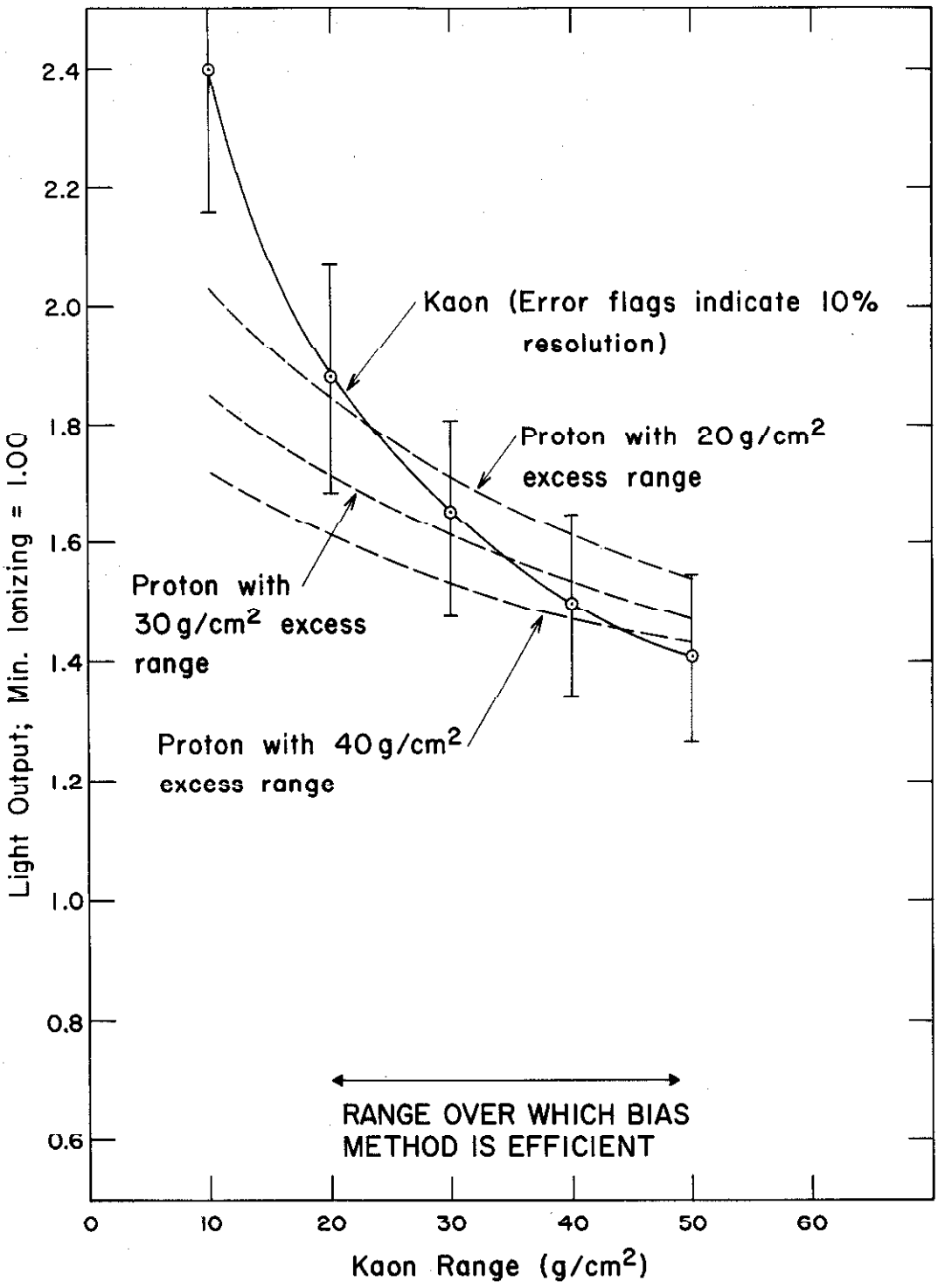

FIGURE 22: A Comparison of the Light Output for Scattering Protons with That Expected for Kaons

This restriction not only limited the number of counters which could be used, but also required that the particle identification be performed where the dL/dx for protons, kaons, and pions were most similar. Furthermore, the bias method could not be expected to reject some fast protons which interacted or scattered later in the telescope.

Therefore, a more detailed fit to the pulse-height data was required. The bias windows could be used to select kaon-like events, which then were analyzed by a digital computer. Because the computer could determine almost exactly where the particle stopped, the more significant dL/dx data near the end of the range of the particle could be used to compute the probability that the particle was a kaon. Also, interacting or scattering protons could be distinguished by large pulses indicating a nuclear star or by their failure to fit a normally stopping kaon in the later part of the telescope. The charged decay particle of the kaon complicated this scheme, but also provided a check on the particle identification.

Originally, it was planned to gather the data for the cross-section measurements without using the A-telescopes. In order to reduce the triggering rate of the Sampling Digitizer to an acceptable level, the proton detection efficiency had to be less than 1%. Using figure 21, eight counters were chosen for bias windows, and a part of the signal from the stopping section was added to the outputs of the front eight scintillators to reduce the effects of range variation. (See section 3.3.) However, because the interaction events were so numerous that the data analysis was unable to eliminate the

background, additional information from the Λ-telescopes was required for clean particle identification. The Λ-telescope coincidence requirement sufficiently reduced the Sampling Digitizer triggering rate so that the bias windows could be set sufficiently wide for the feedback from the stopping section to be unnecessary.

APPENDIX B

Modular Instrumentation System

General

The parts of the general instrumentation system used in this experiment are summarized below. These circuits were designed by Arpad Barna* and myself under the supervision of Professor Matthew Sands.*(18.19)

Amplifiers

1. TA-2. This distributed pulse amplifier(46) has a gain of 10 with a risetime (10% to 90%) of 2.5 ns. It has a 125-ohm input impedance and will deliver up to -2V into a 125-ohm load. The circuit has been constructed both on a copper plate and on the standard size printed circuit board. Presently, it is considered obsolete and is superseded by the TA-8.

2. TA-8. This high-speed pulse amplifier consists of two identical sections with stable amplifications of 3.15 and risetimes of 1.4 ns. When these two sections are cascaded, they provide an amplification of 10 with a risetime of 2 ns up to output voltages of -4V. Outputs as large as -6V may be obtained with a risetime of 2.5 ns. The amplifier, which does not invert, has an input impedance of 125 ohms; the output is intended to drive a 125-ohm resistive load.

Coincidence Circuits

1. TC-2. The details of this multifold coincidence-anticoincidence circuit may be found in reference 22. The circuit accepts

---

* Now at the Stanford Linear Accelerator Center, Stanford University.

pulses less than 10-ns wide, shapes them passively to a critically damped pulse with a 50-ns half-width, and amplifies them by as much as a factor of 250. The amplifier output drives two independent discriminators, the outputs from which may be combined with the outputs of other discriminators in a fast (50 ns to 75 ns) logic circuit. Here various coincidence-anticoincidence combinations may be selected by front panel switches. The outputs of the fast logic circuits may be further combined by the slow logic circuit, or by the TL-4, TL-5, or TL-6, which provide additional coincidence-anticoincidence combinations with resolving times of about 300 ns.

2. TC-3A. This fourfold coincidence-anticoincidence circuit has typical resolving times of 2 to 20 ns, determined by an external clipping cable, and is similar in operation to the circuit of reference 47. Two of the inputs are permanently connected in coincidence, one permanently in anticoincidence, and one can be switched either way. The circuit exhibits stable operation up to a 10% duty cycle of the input pulses (e.g. a maximum average rate of 10^7 pulses per second for 10-ns wide pulses). Because each input is equivalent to a 125-ohm line with a delay of about 1 ns, the inputs of several circuits can be cascaded. The input pulse should be greater than -2V in amplitude. The output is a negative pulse, the width of which is a function of the clipping stub length and which is typically -3V high and 5-ns wide. This output is suitable for driving a subsequent TC-3A (or TC-4) for secondary coincidence operations.

3. TC-4. This coincidence circuit is similar to the TC-3A but has only two coincidence inputs and no anticoincidence provisions.

Gates

1. TG-1A. This fast linear gate, which is constructed on a copper plate, has been described in reference 48. The gate is intended to pass or block photomultiplier tube pulses, which enter at the DC coupled 125-ohm signal input. The gate may be opened or closed by a gating pulse, with a minimum width of 40 ns and a maximum rise time of 15 ns, entering the 125-ohm gate input. Three identical outputs are provided, each designed to drive a 125-ohm load. The circuit operates on signal inputs ranging from -50 mV to -5V, with the gating pulse amplitude being about -2.8V (e.g. the output of the TVD-1A). In typical applications, the circuit has a linearity of ± 1% of full scale and a feedthrough of the input signal of about 0.1%.

2. TG-1B. This fast linear gate[49] is a printed circuit version of the TG-1A and has nearly the same properties as the copper plate model.

Discriminators

1. TVD-1A. This high-speed pulse discriminator operates on pulses from photomultiplier tubes or from the output of fast coincidence-anticoincidence circuits. The input trigger level is adjustable between -0.25V and -5V for 10-ns wide input pulses, with a maximum continuous counting rate of 10 MHz. The pulses from the three main outputs are -3V in amplitude into a 125-ohm load with a width of 50 ns (adjustable by ± 10 ns) and with rise and fall times typically of 12 ns. In addition to the three main outputs,

an auxiliary output provides a 0.5 μs wide pulse with an amplitude of 2.2V.

2. TVD-2. This pulse discriminator provides a 7 μs output pulse intended to drive the digital inputs of the Sampling Digitizer. The discriminator triggers on negative input pulses greater than 1V in amplitude with widths greater than 50 ns. The input may be gated by a negative pulse such as produced by the auxiliary output of the TVD-1A.

Mixing Circuits

1. TDM-4. This linear adding circuit combines the outputs of two photomultiplier tubes, while preventing one of them from influencing the other. The input impedance is 125 ohms, and the output drives a 125-ohm load with a rise time of 2 ns for negative signals less than 3V in amplitude.

2. TDM-5. This pulse mixer adds together 10% of the five inputs. The remaining 90% of each input leaves the circuit with no influence from the other inputs. The input impedances of the five inputs are 125 ohms, when the 90% outputs are loaded by 125 ohms. The sum output drives a 125-ohm load with a rise time of 3 ns for negative inputs less than 3V in amplitude.

APPENDIX C

K Telescope Resolution Function

The cross-section was proportional to an integral over the K-telescope, target, and photon energy. (See section 5.2.) The evaluation of this integral is discussed here.

From equation 14 the integral to be evaluated is:

$$I = \int_{\substack{\text{K-Telescope}\\ \text{Angles}}} \int_{\text{Target}} \int_{\substack{\text{Photon}\\ \text{Energy}}} R_k \frac{B(k, E_o)}{k} \left(\frac{d\sigma}{d\Omega'}\right) dk dz d\Omega_k \quad (18)$$

The geometry and coordinate systems being used are shown in figure 23, with relevant constants being given in table 12.

The telescope was designed[14] so that the angular acceptance would be determined only by the aperture counter and the target. Also, the target, which was a cylinder centered on the photon beam, had a cross-sectional area larger than the area of the collimated beam, making the cross-section measurement independent of the target diameter. Because the RMS beam width of 0.3 inches was small compared to the counter dimensions, the target was approximated by a line source.

The K-telescope resolution function R_k depended on the telescope-target dimensions and on the kaon kinetic energy T_k, and could be factored as follows:

$$R_k = R(T_k)R(\theta, \Phi, z) \quad (19)$$

where: $R(T_k) = 1$ for kaons stopping in the δR counters

TABLE 12

Parameters for the Calculation of I

Target diameter	2 inches
Target length (ℓ)	6.39 inches
Beam cross-sectional area	1×0.8 inches^2
Height of aperture counter (h)	4.0 inches
Width of aperture counter (w)	4.0 inches
Distance of aperture counter from target (r_o)	49 inches
Central angle (θ_o) at:	
E_γ = 1098 MeV	37.36°
E_γ = 1187 MeV	40.17°
E_γ = 1292 MeV	41.48°

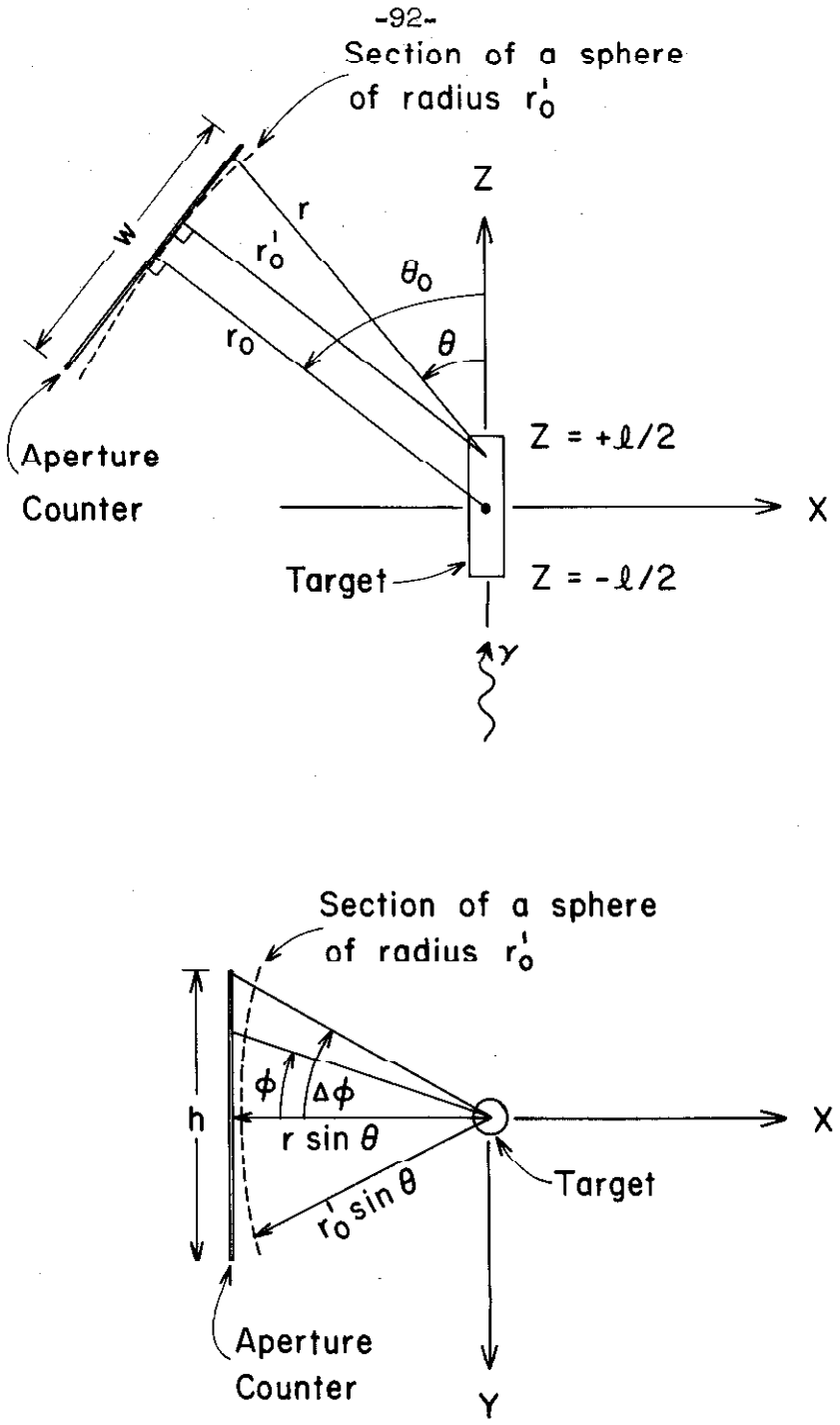

Note: This figure is illustrative only and is not to scale.

FIGURE 23: K-Telescope and Target Geometry

$R(T_k) = 0$ for kaons not stopping in the δR counters

$R(\theta, \Phi, z)$ = geometrical acceptance of the target-telescope system.

The kaon kinetic energy and angle, and the photon energy are related by $K\Lambda$ photoproduction kinematics, which were tabulated by an IBM 7094 computer. The geometrical acceptance was calculated as follows.

For a fixed point z on the target,

$$d\Omega_k = \sin\theta d\theta d\Phi \tag{20}$$

and the integral over Φ can be trivially performed, yielding:

$$R(\theta, z) = \int_{-\Delta\Phi}^{+\Delta\Phi} R(\theta, \Phi, z) d\Phi = 2 \left[\cot^{-1} \left(\frac{2r \sin\theta}{h} \right) \right] \tag{21}$$

Then, integrating over the target gives:

$$R(\theta) = \int_{Z_{min}}^{Z_{max}} R(\theta, z) dz = 2 \int_{Z_{min}}^{Z_{max}} \cot^{-1} \left[\frac{2(r_o - z \cos\theta_o)\sin\theta}{h \cos(\theta_o - \theta)} \right] dz \tag{22}$$

where: Z_{min} = larger of $\left[-\frac{\ell}{2}, (r_o \cos\theta_o - \frac{\omega}{2} \sin\theta_o) - (r_o \sin\theta_o + \frac{\omega}{2} \cos\theta_o) \cot\theta \right]$

Z_{max} = smaller of $\left[\frac{\ell}{2}, (r_o \cos\theta_o + \frac{\omega}{2} \sin\theta_o) + (-r_o \sin\theta_o + \frac{\omega}{2} \cos\theta_o) \cot\theta \right]$

This integral can be evaluated exactly giving:

$$R(\theta) = \frac{-h \cos(\theta_o - \theta)}{\cos \theta_o \sin \theta} \left\{ S \cot^{-1} S + \frac{1}{2} \ln (1 + S^2) \right\} \Bigg|_{S_1}^{S_2} \qquad (23)$$

where: $S = \dfrac{2(r_o - z \cos \theta_o) \sin \theta}{h \cos (\theta_o - \theta)}$

$$S_1 = S(Z_{min})$$

$$S_2 = S(Z_{max})$$

Expanding to second order in h/r_o and z/r_o, $R(\theta)$ reduces to:

$$R(\theta) = \frac{h \cos (\theta_o - \theta)}{r_o \sin \theta} \left[(Z_{max} - Z_{min}) + \frac{(Z_{max}^2 - Z_{min}^2) \cos \theta_o}{2 r_o} \right] \qquad (24)$$

with the errors resulting from the approximations being less than 0.3%.

The integrals over telescope angles and over the target have now been reduced to:

$$I = \int_{\theta} \int_{\substack{\text{Photon} \\ \text{Energy}}} \frac{R(T_k) R(\theta) B(k, E_o) \sin\theta}{k} \left(\frac{d\Omega}{d\Omega}\right) dk \, d\theta \qquad (25)$$

where $R(\theta)$ is given by equation 24 for positive values of $R(\theta)$. Otherwise, $R(\theta)$ is zero. The regions over which $R(\theta)$ is not zero are cross-hatched in figure 24. Four boundary angles are relevant — namely:

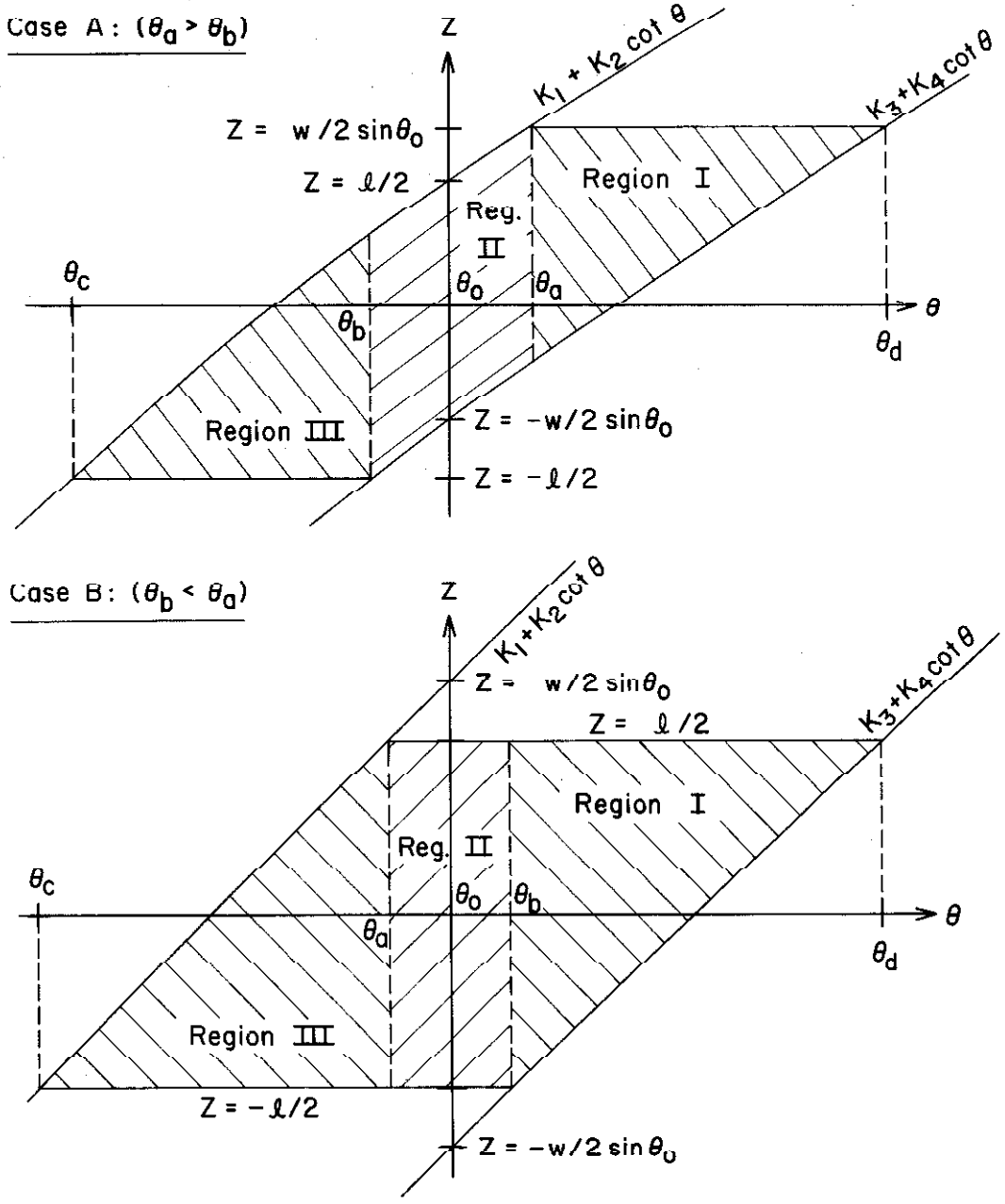

Note: This figure is illustrative only and is not to scale.

FIGURE 24: Regions Over Which $R(\theta)$ is Not Zero

$$\theta_a = \cot^{-1}\left(\frac{\frac{\ell}{2} - K_1}{K_2}\right) \tag{26}$$

$$\theta_b = \cot^{-1}\left(\frac{-\frac{\ell}{2} - K_3}{K_4}\right)$$

$$\theta_c = \cot^{-1}\left(\frac{-\frac{\ell}{2} - K_1}{K_2}\right)$$

$$\theta_d = \cot^{-1}\left(\frac{\frac{\ell}{2} - K_3}{K_4}\right)$$

where: $K_1 = r_o \cos\theta_o + \frac{\omega}{2}\sin\theta_o$

$K_2 = -r_o \sin\theta_o + \frac{\omega}{2}\cos\theta_o$

$K_3 = r_o \cos\theta_o - \frac{\omega}{2}\sin\theta_o$

$K_4 = -r_o \sin\theta_o - \frac{\omega}{2}\cos\theta_o$

Two cases need to be considered – case A where $\theta_a > \theta_b$ and case B where $\theta_b > \theta_a$. Both cases are shown in figure 24.

In each of the regions, $R(\theta)$ was expanded in a power series to second order about one of the boundary angles. The integration could then be trivially performed for each region "i", yielding:

$$F_i(\delta_i) = \int_o^{\delta_i} R(\delta_i)\sin(\delta_i + \theta_i)\, d\delta_i \tag{27}$$

$$\cong (M_i\delta_i + N_i\delta_i^2 + P_i\delta_i^3)\, 2.54$$

where: $\delta_i = \theta - \theta_i$

θ_i = appropriate boundary angle

M_i, N_i, P_i = constants determined by the expansion and integration.

Values for the above quantities are given in table 13. (The factor of 2.54 converts from inches to centimeters.) The constants were calculated from the following formulae:

REGION I CASE A or B

$$\theta_1 = \theta_d$$

$$M_1 = 0 \tag{28a}$$

$$N_1 = \frac{h}{2r_o}\left[\cos(\theta_o-\theta_d)\right]\left[1+\frac{\ell\cos\theta_o}{2r_o}\right]\frac{K_4}{\sin^2\theta_d}$$

$$P_1 = \frac{-h}{3r_o}\left\{\left[\cos(\theta_o-\theta_d)\right]\left[\left(1+\frac{\ell\cos\theta_o}{2r_o}\right)\left(K_4\cot^3\theta_d\right)+\left(\frac{\cos\theta_o}{2r_o}\right)\left(\frac{K_4}{\sin^2\theta_d}\right)^2\right]+\left[\sin(\theta_o-\theta_d)\right]\left[1+\frac{\ell\cos\theta_o}{2r_o}\right]\left[\frac{K_4}{\sin^2\theta_d}\right]\right\}$$

REGION II - CASE A

$$\theta_2 = \theta_b$$

$$M_2 = \frac{h\omega}{r_o\sin\theta_o} \tag{28b}$$

$$P_2 \cong 0$$

REGION II - CASE B

$$\theta_2 = \theta_a$$

$$M_2 = \frac{\ell h}{r_o} \tag{28c}$$

$$P_2 \cong 0$$

TABLE 13

Values for F_i

θ_o (degrees)	37.36	40.17	41.48
θ_o (radians)	0.6521	0.7010	0.7242
θ_b (radians)	0.6534	0.6993	0.7229
θ_c (radians)	0.5757	0.6230	0.6433
θ_d (radians)	0.7373	0.7883	0.8132
T_{ko} (MeV)	179	234	288
$T_{ko} + \Delta T_k$ (MeV)	197.8	250.7	303.6
$T_{ko} - \Delta T_k$ (MeV)	160.2	217.3	272.4
REGION I			
θ_1 (radians)	0.7373	0.7883	0.8132
M_1 (inches - radians)	0	0	0
N_1 (inches)	2.96	2.81	2.74
P_1 (inches/radian)	-0.31	-0.173	-0.124
REGION II	CASE B	CASE A	CASE A
θ_2 (radians)	0.6517	0.6993	0.7229
M_2 (inches-radians)	0.521	0.506	0.493
N_2 (inches)	0	0	0
P_3 (inches/radian)	~0	~0	~0
REGION III			
θ_3 (radians)	0.5757	0.6230	0.6433
M_3 (inches-radians)	0	0	0
N_3 (inches)	3.65	3.42	3.33
P_3 (inches/radian)	-0.475	-0.258	-0.153

REGION III - CASE A or B

$$\theta_3 = \theta_c$$

$$M_3 = 0$$

$$N_3 = \frac{-h}{2r_o} \cos\left[(\theta_o - \theta_c)\right]\left[1 - \frac{\ell \cos\theta_o}{2r_o}\right] \frac{K_2}{\sin^2\theta_c}$$

$$P_3 = \frac{h}{3r_o}\left\{\left[\cos(\theta_o - \theta_c)\right]\left[\left(1 - \frac{\ell \cos\theta_o}{2r_o}\right)(K_2\cot^3\theta_c)\right.\right.$$

$$\left. + \left(\frac{\cos\theta_o}{2r_o}\right)\left(\frac{K_2}{\sin^2\theta_c}\right)^2\right]$$

$$\left.\left[\sin(\theta_o - \theta_c)\right]\left[1 - \frac{\ell \cos\theta_o}{2r_o}\right]\left[\frac{K_2}{\sin^2\theta_c}\right]\right\}$$

Because typically the third order term contributed about 0.5% to the integral and never more than 1%, this term was neglected in further computations.

For a given photon energy, the $K\Lambda$ photoproduction kinematics, the restricted particle range and the boundary angles defined a range of angles for which a kaon would have an acceptable kinetic energy and a laboratory angle lying in a given region. The integral over photon energy could thus be written:

$$I = \int_o^{E_o} \frac{B(k, E_o)}{k} \sum_{i=1}^{3} \frac{\Delta F_i(k)}{\left(\frac{d\Omega'}{d\Omega}\right)}\, dk \qquad (29)$$

where the summation was over the three angle regions and $\frac{d\Omega'}{d\Omega}$ was averaged over the kaon direction for fixed k. The angle functions $\Delta F_i(k)$ are given by:

$$\Delta F_1 = 2.54\, N_1 \left\{ \left[\theta_{21}(k) - \theta_d\right]^2 - \left[\theta_{11}(k) - \theta_d\right]^2 \right\} \qquad (30a)$$

$$\Delta F_2 = 2.54\, M_2 \left\{ \theta_{22}(k) - \theta_{12}(k) \right\} \qquad (30b)$$

$$\Delta F_3 = 2.54\, N_3 \left\{ \left[\theta_{23}(k) - \theta_c\right]^2 - \left[\theta_{13}(k) - \theta_c\right]^2 \right\} \qquad (30c)$$

where: $\theta_{1i}(k)$ = the angle at which $T_k = T_{ko} + \Delta T_k$ for a photon energy k, but equal to the nearest boundary angle for region "i" if otherwise $\theta_{1i}(k)$ would be outside of region "i".

$\theta_{2i}(k)$ - The angle at which $T_k = T_{ko} - \Delta T_k$ for a photon energy k, but equal to the nearest boundary angle for region "i" if otherwise $\theta_{2i}(k)$ would be outside of region "i".

T_k = kaon kinetic energy.

The integrand in equation 29 was evaluated at 10 MeV increments of photon energy and provided the energy resolution function in figure 18. The evaluation of the integral resulted in the quantity "I" used in the reduction of the cross-section data. The theoretical excitation curves of figure 19 were calculated from equations 29 and 30 by varying E_o.

The angular resolution function was obtained by integrating over photon energy before integrating over angle. With this approach

equation 29 can be rewritten:

$$I = \int_{\theta_c}^{\theta_d} G(\theta, \theta_o E_o) d\theta \tag{31}$$

where in region I: $G = 2N_1(\theta_d - \theta)\, H(\theta, E_o)$

in region II: $G = M_2 H(\theta, E_o)$

in region III: $G = 2N_3(\theta - \theta_c) H(\theta, E_o)$

The integral over photon energy provided $H(\theta, E_o)$ as follows:

$$H(\theta, E_o) = \int_{k_1(\theta)}^{k_2(\theta)} \frac{B(k, E_o)dk}{k \quad (\frac{d\Omega'}{d\Omega})} \tag{32}$$

where: $k_2(\theta)$ = photon energy for which $T_k = T_{ko} + \Delta T_k$ at a kaon angle of θ.

$k_1(\theta)$ = photon energy for which $T_k = T_{ko} - \Delta T_k$ at a kaon angle of θ.

The angular resolution functions shown in figure 17 represent a plot of $G(\theta, \theta_o, E_o)$.

REFERENCES

1. P. L. Donoho and R. L. Walker, Phys. Rev. 107, 1198 (1957).

2. P. L. Donoho and R. L. Walker, Phys. Rev. 112, 981 (1958).

3. A. Silverman, R. R. Wilson, and W. M. Woodward, Phys. Rev. 108, 501 (1957).

4. H. M. Brody, A. M. Wetherell, and R. L. Walker, Phys. Rev. 110, 1213 (1958).

5. H. M. Brody, A. M. Wetherell, and R. L. Walker, Phys. Rev. 119, 1710 (1960).

6. B. D. McDaniel, A. Silverman, R. R. Wilson, and G. Cortellessa, Phys. Rev. Lett. 1, 109 (1958).

7. B. D. McDaniel, A. Silverman, R. R. Wilson, and G. Cortellessa, Phys. Rev. Lett. 1, 109 (1958).

8. R. L. Anderson, E. Gabathuler, B. D. McDaniel and A. J. Sudoff, Phys. Rev. Lett. 9, 131 (1962).

9. H. Thom, E. Gabathuler, D. Jones, B. D. McDaniel, and W. M. Woodward, Phys. Rev. Lett. 11, 433 (1963).

10. C. W. Peck, Phys. Rev. 135, B830 (1964).

11. M. D. Daybell, Ph.D. Thesis, California Institute of Technology, 1962 (unpublished).

12. M. Ernstene, Ph.D. Thesis, California Institute of Technology, 1959 (unpublished).

13. D. E. Groom and J. H. Marshall, Bull. Am. Phys. Soc. 10, 79 (1965).

14. D. E. Groom, Ph.D. Thesis, California Institute of Technology, 1965 (unpublished).

15. D. E. Groom and J. H. Marshall, Rev. Sci. Inst. 33, 1249 (1962).

16. J. H. Marshall, "Synchrotron 220 Data Channel Operating Instructions and Specifications" (unpublished).

17. D. E. Groom, "KERN Instruction Manual" (unpublished).

18. A. Barna, J. H. Marshall and D. Torzewski, Rev. Sci. Inst. 36, 1666 (1965).

19. A. Barna and D. Torzewski, "Modular Instrumentation Handbook," EFINS 63-83 (Part I, 1963) and EFINS 64-66 (Part II, 1964).

20. C. W. Peck, Ph.D. Thesis, California Institute of Technology, 1964 (unpublished).

21. A. Barna, Nucl. Instr. Methods 24, 247 (1963).

22. A. Barna, J. H. Marshall and M. Sands, Nucl. Instr. Methods 12, 43 (1961).

23. J. H. Marshall, "Master Control Instruction Manual" (unpublished).

24. D. E. Groom and M. G. Hauser, "A Note on the Light Output-Energy Loss Relationship for Plastic Scintillator NE-102," 1965 (to be published).

25. A. Barna and J. H. Marshall, "Transistor Circuit Reliability at the Caltech Synchrotron," 1961 (unpublished).

26. R. R. Wilson, Nucl. Instr. Methods 1, 101 (1957).

27. D. E. Groom, "Decay Particle Corrections in a K^+ Range Telescope," private communication.

28. J. E. Lannutti, S. Goldhaber, G. Goldhaber, W. W. Chupp, S. Giambuzzi, C. Marchi, G. Quareni, and A. Wataghin,

Phys. Rev. 109, 2121 (1958).

29. T. F. Kycia, L. T. Kerth, and R. G. Baender, UCRL-8753.

30. L. T. Kerth, T. F. Kycia, and L. van Rossum, Phys. Rev. 109, 1784 (1958).

31. S. Hatsukade and H. J. Schnitzer, Phys. Rev. 128, 468 (1962).

32. S. Hatsukade and H. J. Schnitzer, Phys. Rev. 132, 1301 (1963).

33. M. Gourdin and J. Dafour, Nuovo Cimento 27, 1410 (1963).

34. J. Dufour, Nuovo Cimento 34, 5693 (1964).

35. T. K. Kuo, Phys. Rev. 129, 2264 (1963).

36. N. A. Beauchamp and W.G. Holliday, Phys. Rev. 131, 2719 (1963).

37. J. Dufour, private communication (1965).

38. S. Coleman and S. L. Glashow, Phys. Rev. Lett. 6, 423 (1961).

39. R. L. Cool, E. W. Jenkins, T. F. Kycia, D. A. Hill, L. Marshall and R. A. Schulter, Phys. Rev. 127, 2223 (1962).

40. W. Kerman, T. B. Novcy, S. D. Warshaw, and A. Wattenburg, Phys. Rev. 129, 870 (1963).

41. "A Compendium of Properties of Materials at Low Temperature," Wright Air Development Division, Air Research and Development Command, USAF - V. J. Johnson, Editor.

42. A. H. Rosenfeld, A. Barbaro - Galtieri, W. H. Barkas, P. L. Bostien, J. Kirz and M. Roos, Rev. Mod. Phys. 36, 977 (1964).

43. Glasstone, "Elements of Physical Chemistry," (1946).

44. F. Wolverton, "Thick Radiator Bremsstrahlung. Angular Dependence of the Spectrum for Electron Energies Greater

Than 300 MeV," 1965 (to be published).

45. K. Symon, Ph.D. Thesis, Harvard University, 1948 (unpublished).

46. A. Barna and J. H. Marshall, CTSL-27 (1961).

47. A. Barna, J. H. Marshall, and M. Sands, Nucl. Instr. Methods 7, 124 (1960).

48. A. Barna and J. H. Marshall, CTSL - 18 (1961).

49. A. Barna and J. H. Marshall, Rev. Sci. Instr. 35, 881 (1964).